



Vehicles Dynamics, Planning and Control of Robotic Cars

Final Report

Basem Shaker <basem.shaker@studenti.unitn.it>

Presented to: Gastone Pietro Rosati Papini

June 2022

Contents

| | |
|---|-----------|
| 1 Tire Model Exercises - 1 | 2 |
| 1.1 Exercise 1 – Pure Longitudinal Slip | 2 |
| 1.2 Exercise 2 - Combined Slip | 5 |
| 2 Tire Model Exercises - 2 | 7 |
| 2.1 Exercise 1 – Understanding Tire Data | 7 |
| 2.2 Exercise 2 - Fitting Tire Data | 9 |
| 3 Vehicle Data Analysis Exercises | 12 |
| 3.1 Exercise 1 – Understanding Vehicle Data | 12 |
| 4 Vehicle Model Exercises | 16 |
| 4.1 Exercise 1 - Vehicle Model Implementation | 16 |
| 5 Handling Identification | 24 |
| 5.1 Exercise 1 - Sine Steer Maneuvers | 24 |
| 5.2 Exercise 2 - Constant Steer Maneuvers | 30 |
| 6 Lateral Control | 35 |
| 6.1 Exercise 1 - lateral control | 35 |
| 7 Motion Planning and Control | 45 |
| 7.1 Exercise 1 - route planning | 45 |
| 7.2 Exercise 2 - lateral control | 53 |

Assignment 1

Tire Model Exercises - 1

1.1 Exercise 1 – Pure Longitudinal Slip

Q. Using the Pacejka Magic Formula, plot the longitudinal tire force F_{x0} obtained in pure longitudinal slip conditions, as a function of slip $\kappa \in [-1, 1]$. Which comments are you able to make about the obtained graph?

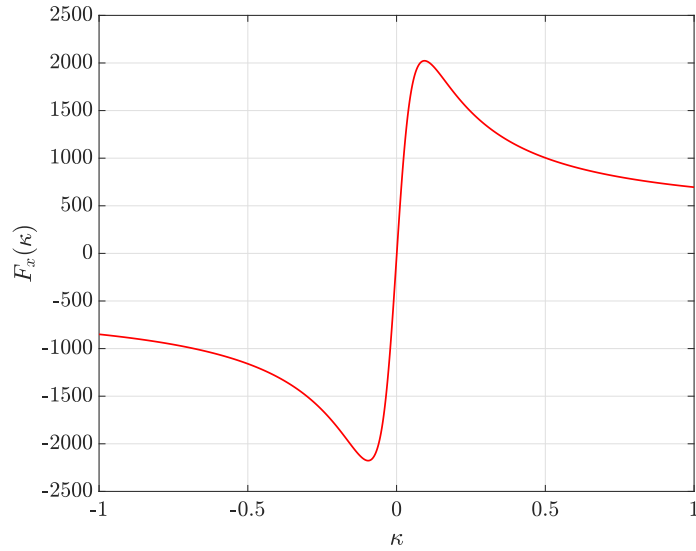


Figure 1.1: F_{x0} as a function of slip

When κ (longitudinal slip) increases, F_x grows until it reaches a saturation limit. Furthermore, the slip zone grows, and the adherence area decreases. That means, the total tire

force F_x keeps growing until it reaches a peak and a saturation limit as shown in Figure 1.2. κ (longitudinal slip) is positive when the tire is accelerating, negative during braking, and reaches -1 when the wheel locks.

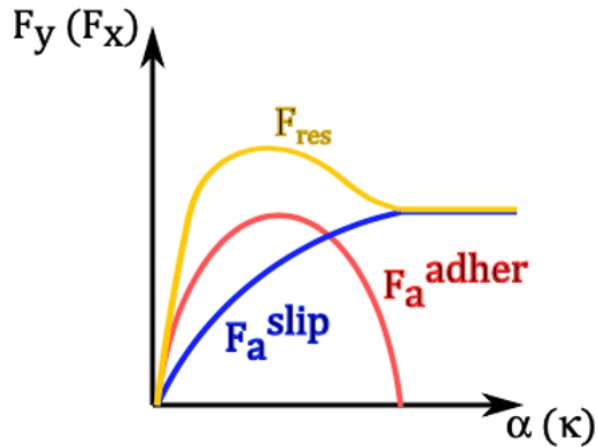


Figure 1.2: Slip and adherence forces

Q. If you were supposed to design a traction control system for maximizing vehicle longitudinal acceleration, which would be the target value of longitudinal slip κ that you would try to achieve?

Acceleration is directly proportional to the force [$F=ma$] if the mass is constant. If I want to maximize the vehicle longitudinal acceleration, I would need to maximize the longitudinal force [F_x]. F_x is highest at the saturation limit, which in this example happens at slip $\kappa = 0.094$, and yields an F_x of 2022.99 N.

Q. Assuming that wheel rotational speed is $\omega = 70$ rad/s, tire effective rolling radius is $R_e = 0.2$ m, while the longitudinal component of tire contact point speed $v_{Cx} = 13$ m/s, compute the longitudinal slip κ . In these conditions, is the wheel accelerating, braking or is it in pure rolling? Compute also the corresponding longitudinal tire force F_{x0}

Using Matlab, the calculated longitudinal slip $\kappa = 0.0769$ and the calculated longitudinal force F_x is = 1990.65 N. the longitudinal slip is positive (>0), which means that the wheel is accelerating.

Q. Compute the cornering stiffness Cf_κ , that is the derivative for $\kappa = 0$ of the F_{x0} . Up to which value of κ is the linear approximation of Pacejka curve acceptable?

Assignment 1 – Tire Model Exercises - 1

The cornering stiffness Cf_κ is equal to the derivative of the longitudinal force with respect to the longitudinal slip when the longitudinal slip is equal to zero. This means its equal to the slope at the origin ($x=y=0$) or equal to BCD function as shown in Figure 1.3. The calculated cornering stiffness is $Cf_\kappa = 47909.4$

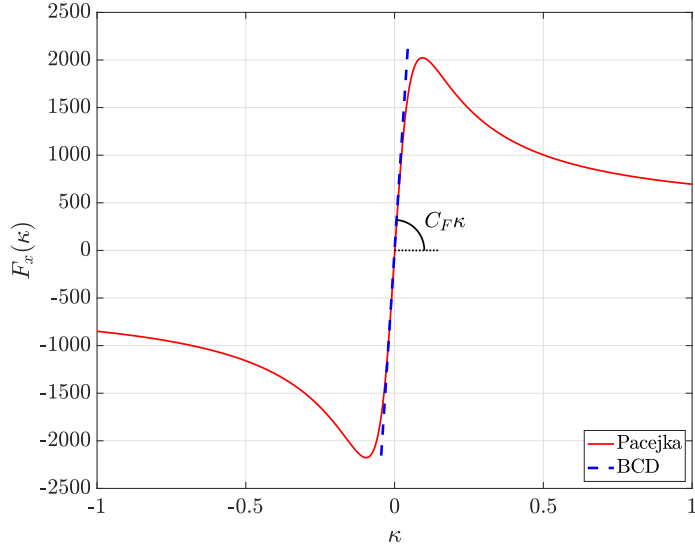


Figure 1.3: cornering stiffness as a linear approximation

The linear approximation allows to neglect the complex Pacejka Magic Formula, but it is valid only for small κ . At $\kappa = 0.02$, the percent difference is already at 10% as shown in Figure 1.4.

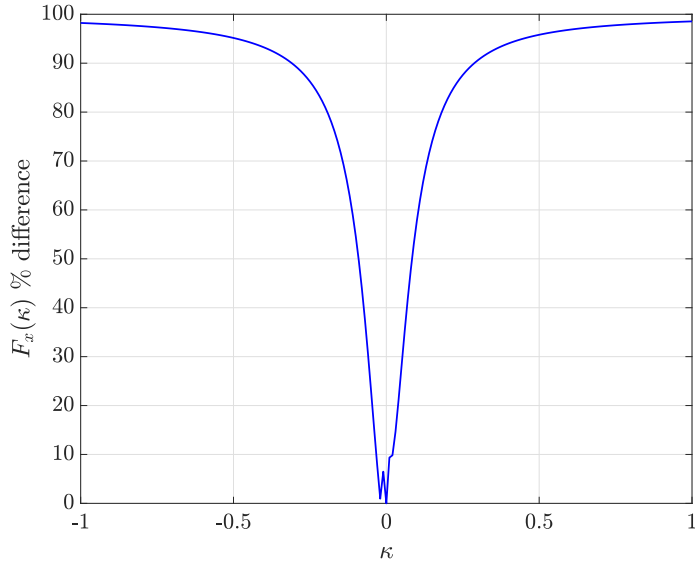


Figure 1.4: % difference in κ using linear approximation vs Pacejka formula

1.2 Exercise 2 - Combined Slip

Q. Assume that the tire contact point velocity components along the tire x and y axes are $v_{Cx} = 15 \text{ m/s}$ and $v_{Cy} = -1.3 \text{ m/s}$, respectively. Calculate the side slip angle α . Moreover, compute the combined tire force F_x using this value of α , for a longitudinal slip $\kappa = 0.08$.

Side slip angle α can be calculated using the practical slip approach:

$$\text{side slip angle } \alpha = -\arctan\left(\frac{v_{sy}}{v_{Cx}}\right) = -\arctan\left(\frac{v_{Cy}}{v_{Cx}}\right) \quad (1.1)$$

Using equation 1.2 to calculate G_{xa} (weighing function). Once calculated, F_{x0} can now be multiplied by G_{xa} (weighing function) to get the combined tire force F_x .

$$G_{xa} = -D_{xa} \cos(C_{xa} \arctan(B_{xa}(\alpha + S_{Hxa}))) \quad (1.2)$$

$$F_{x0} = D_x \sin(C_x \arctan(B_x \kappa_x - E_x(B_x \kappa_x - \arctan(B_x \kappa_x)))) \quad (1.3)$$

$$F_x = G_{xa} F_{x0} \quad (1.4)$$

Using Matlab to calculate the side slip angle α and combined tire force:

calculated side slip $\alpha = 0.086451$
 calculated weighing function $G_{xa} = 0.724417$
 calculated combined force $F_x = 1450.424623$

Q. Plot the combined longitudinal tire force F_x as a function of $\kappa \in [-1, 1]$, for the following levels of side slip angle $\alpha = \{0, 2, 4, 6, 8\}$ degrees. Which comments can you make about the 5 curves obtained in this way? Finally, plot the weighting function G_{xa} as a function of $\kappa \in [-1, 1]$ for each of the previously defined values of α , and briefly comment also these 5 curves.

Figure 1.5 shows plots obtained for the combined longitudinal force F_x for each side slip angle as a function of the longitudinal slip κ . The maximum combined longitudinal force F_x keeps decreasing with higher side slip α .

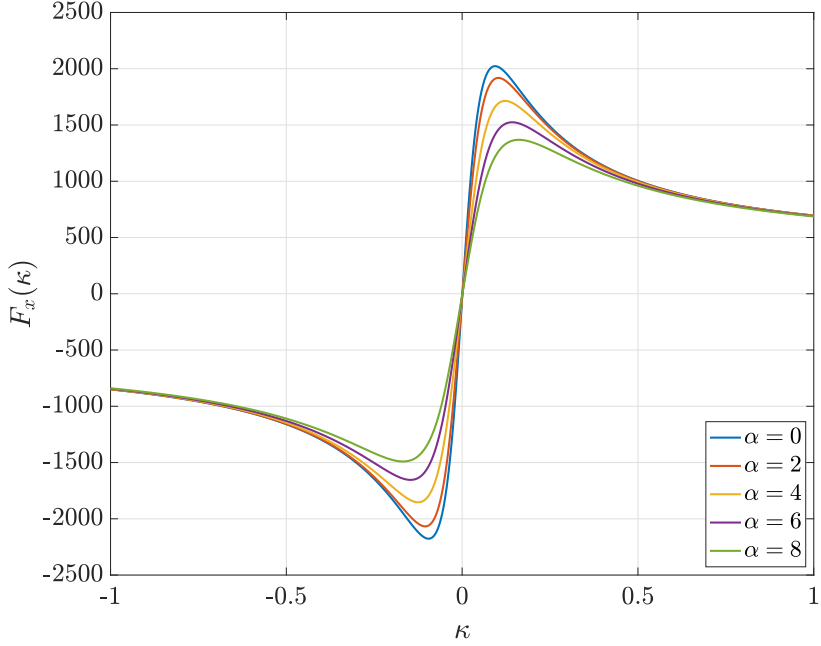


Figure 1.5: combined longitudinal force F_x as a function of κ

Figure 1.6 shows the plots obtained for the weighing function G_{xa} for each side slip angle as a function of the longitudinal slip κ . Higher side slip α decreases the weighing function, which in effect decreases the combined longitudinal force F_x . The effect of the weighing function is quite more potent around $\kappa = 0$, and that effect decreases the further away we are from it.

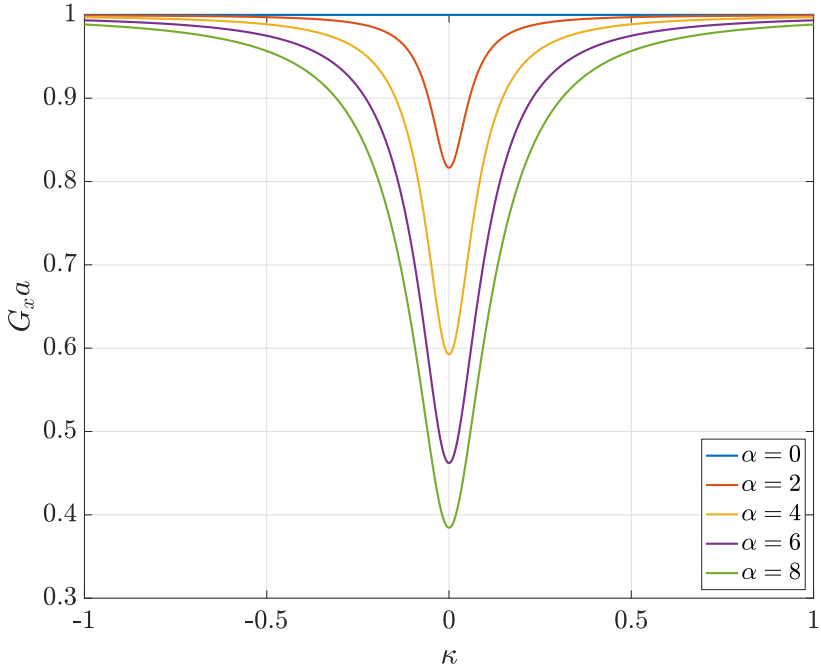


Figure 1.6: Weighing function G_{xa} as a function of κ

Assignment 2

Tire Model Exercises - 2

2.1 Exercise 1 – Understanding Tire Data

Q. Plot the raw data in different graphs, specifically focusing on κ , α , γ , F_z and pressure P . Comment on what you see. What is, according to you, the main target of these tests?

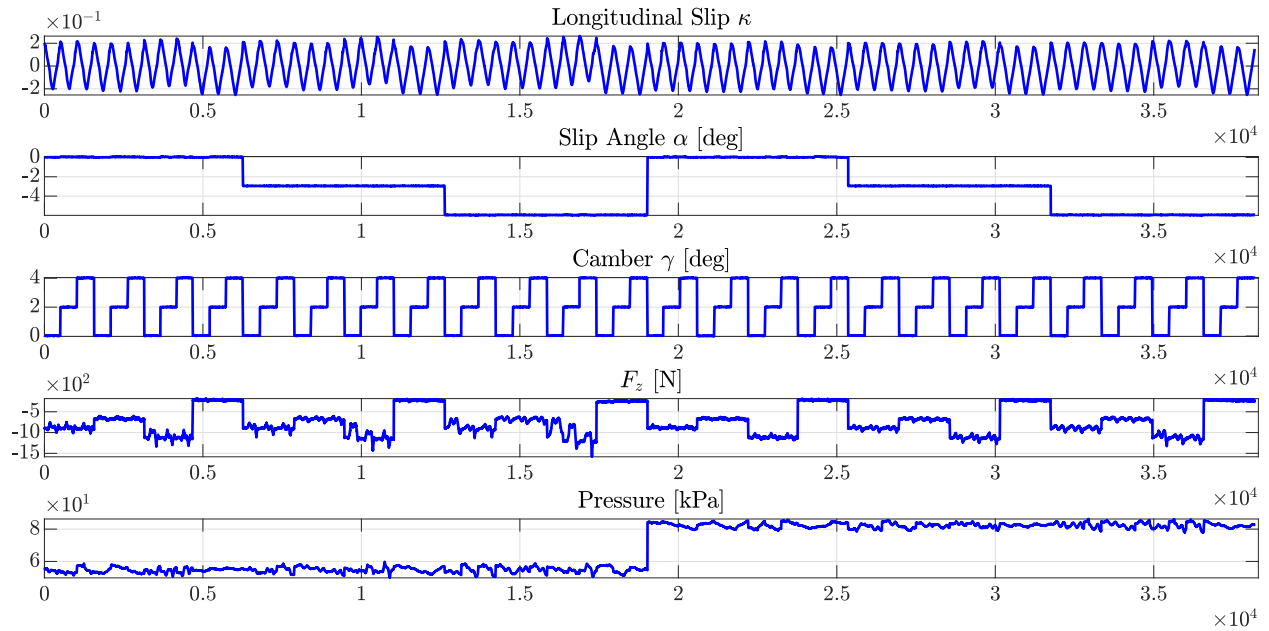


Figure 2.1: raw data

From the five plotted variables in Figure 2.1, it appears that the longitudinal slip, slip angle,

camber, vertical force, and pressure are all showing repeat patterns. That means that those five variables are controlled to measure and test their effect on the longitudinal force F_x . Note that the longitudinal slip κ for each test spanned from 0.2 to -0.2 and then back again to 0.2. The data extracted for the following questions only took the first half of each separate test. Furthermore, only data that had $P = 83$ kPa were used, because the data seemed noisier with $P = 55$ kPa, especially with F_z data.

Q. Focus on the data with $\alpha = 0$ and $\gamma = 0$, and plot the curves F_x vs κ for each of the 4 vertical loads F_z used in the experiments. Plot the 4 curves on the same graph, with different colors. Comment on what you see.

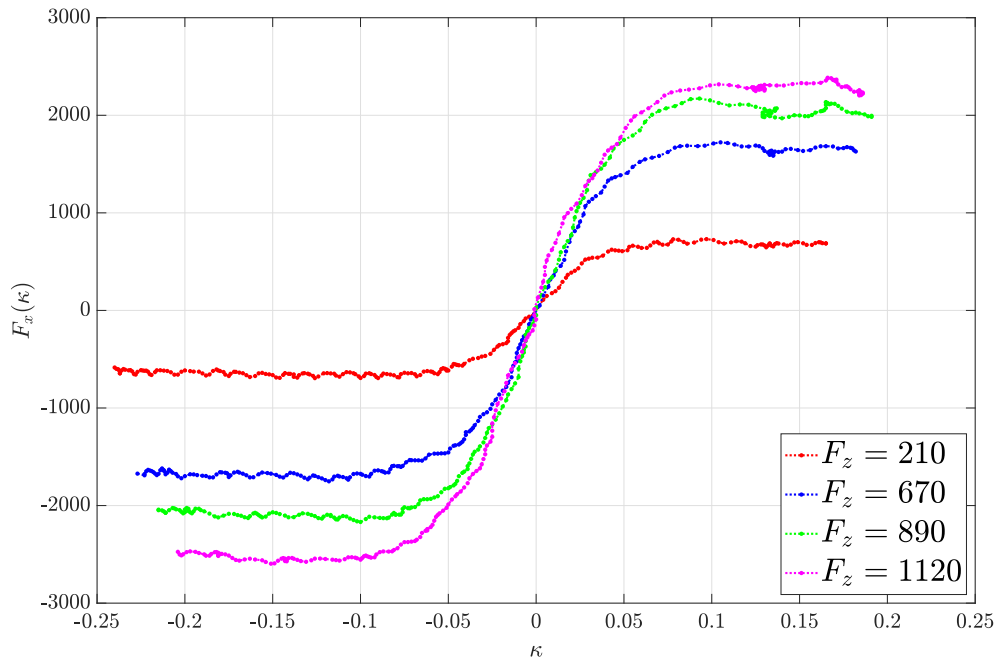


Figure 2.2: κ vs F_x based on vertical force

Figure 2.2 suggests that the Longitudinal Force F_x increases with the vertical force F_z . There is some dependency on the vertical force. If you double the vertical force, it does not mean the longitudinal force will double. In some parts there is a linear dependency, but in others it is not the case.

Q. Focus on the data with $\gamma = 0$ and $F_z = 150$ lbf ≈ 670 N, and plot the curves F_x vs κ for each of the 3 side slip angles α used in the experiments. Plot the 3 curves on the same graph, with different colors. Comment on what you see.

The Longitudinal Force F_x in Figure 2.3 shows an inverse relationship with the side slip angle.

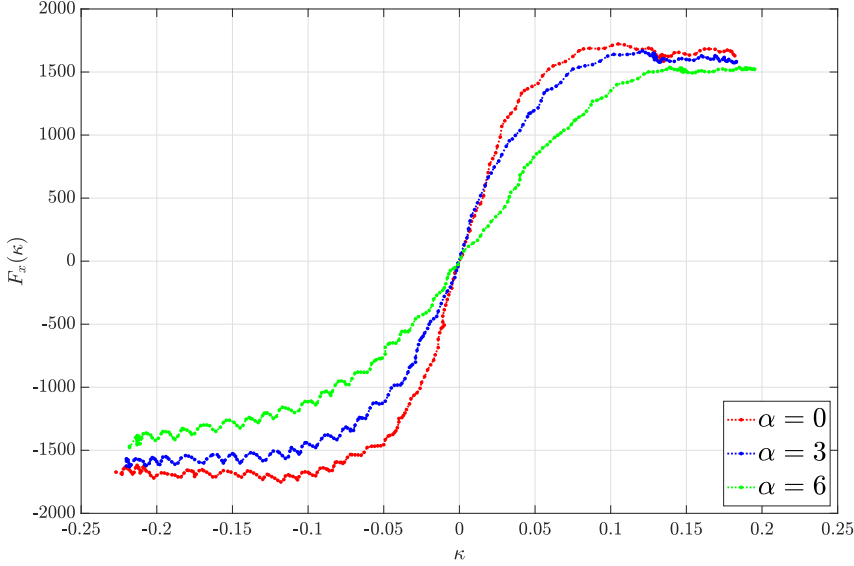


Figure 2.3: κ vs F_x at vertical force = 670 based on slip angle

2.2 Exercise 2 - Fitting Tire Data

Q. First consider the data with $F_z = F_{z0} = 890\text{N}$, $\gamma = 0$ and $\alpha = 0$, and fit the coefficients $\mathbf{X1} = \{p_{Cx1}, p_{dx1}, p_{Ex1}, p_{Ex4}, p_{Kx1}, p_{Hx1}, p_{Vx1}\}$. Plot the fitted curve F_x vs κ that you obtained in these nominal conditions, together with the raw data.

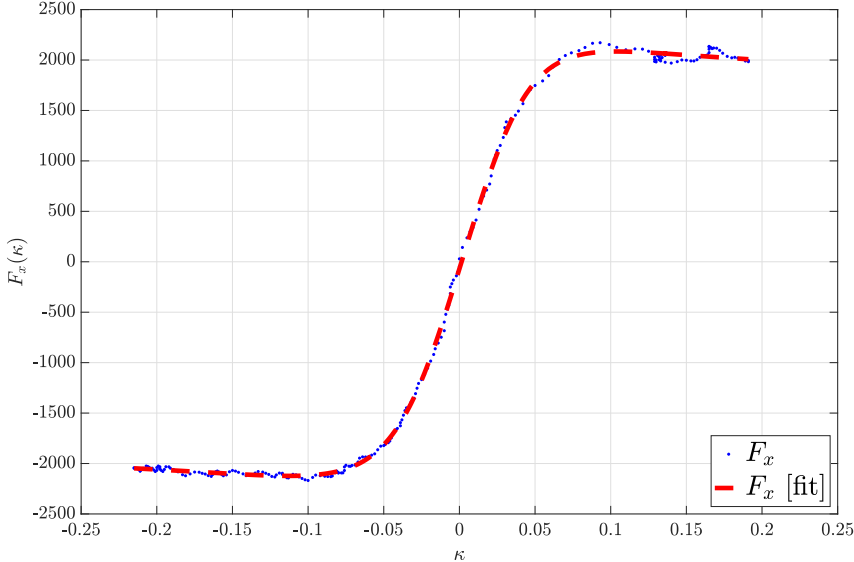


Figure 2.4: Fitted F_{x0} after optimizing first 7 parameters compared to test data vs κ

In Figure 2.4, the data was filtered based on the following criteria: $F_{z0} = 890$, $\alpha = 0$, $\gamma = 0$. The first 7 coefficients were optimized using the *fmincon* function in Matlab. I started with

a random coefficients initial guess vector. The initial guess vector has proven to be quite important as running the code multiple times showed a curve that did not fit the data at all, which means the optimizer was stuck at a local minima. However, most of the time the initial guess gave a very good fit that converged to the correct global minima. Later on I optimized the initial guesses to give consistent good fitting results based on trial and error.

Q. Consider data with the 4 different values of F_z , but still $\gamma = 0$ (and $\alpha = 0$). This enables the fitting of the parameters: $\mathbf{X2} = \{p_{dx2}, p_{Ex2}, p_{Ex3}, p_{Hx2}, p_{Kx2}, p_{Kx3}, p_{Vx2}\}$. Plot fitted and raw curves $F_x(\kappa)$ vs κ for the 4 values of F_z and comment the results.

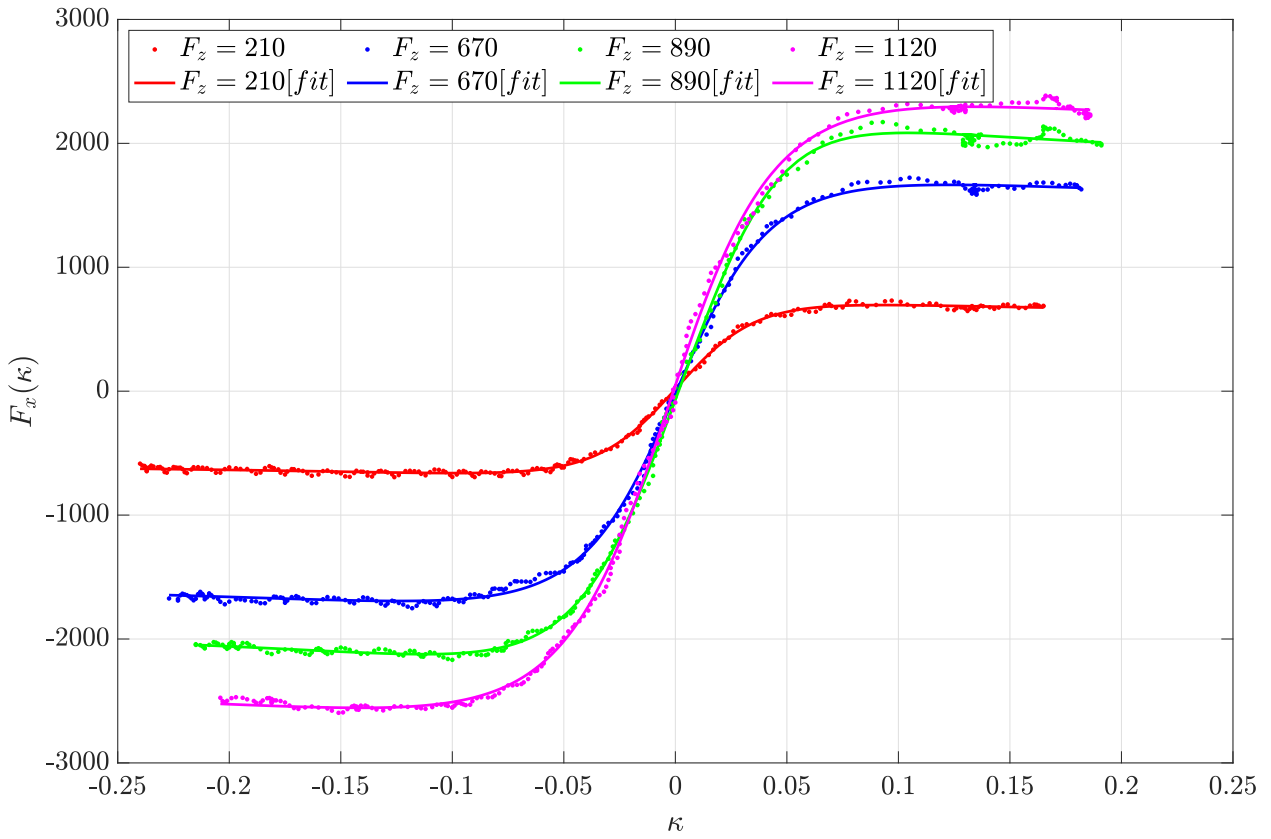


Figure 2.5: Fitted F_x vs test data after second fitting for each F_z

The real F_x data for each separate F_z are plotted against the output of the second fitting in Figure 2.5. The fitted data appear to match the test data quite well. This means the fitting results are adequate to approximate the longitudinal force F_x for vertical forces F_z that are different from the one originally tested.

Q. Now consider the data with the 3 different values of γ , but with $F_z = F_{z0}$ (and $\alpha = 0$). Plot the fitted and raw curves F_{x0} vs κ for the 3 values of γ and comment the results.

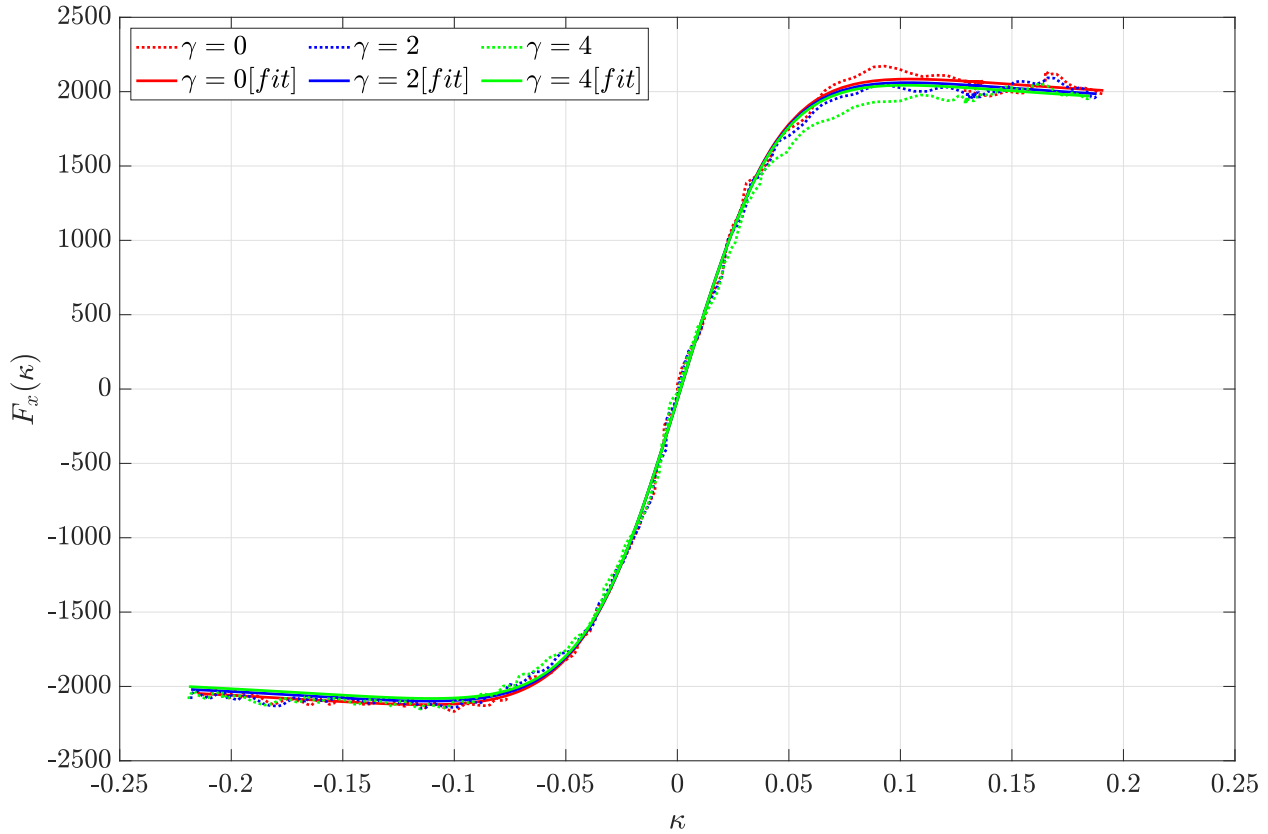


Figure 2.6: Fitted F_x vs test data after third fitting for each γ

Figure 2.6 shows the results of the third fitting. The data from $\gamma = 0$ fits properly as shown previously in Figure 2.4. However, the fitting on the other γ values did not match completely. Trying different initial values for p_{dx2} did not yield any better results.

Assignment 3

Vehicle Data Analysis Exercises

3.1 Exercise 1 – Understanding Vehicle Data

Q. Plot lateral and longitudinal velocity

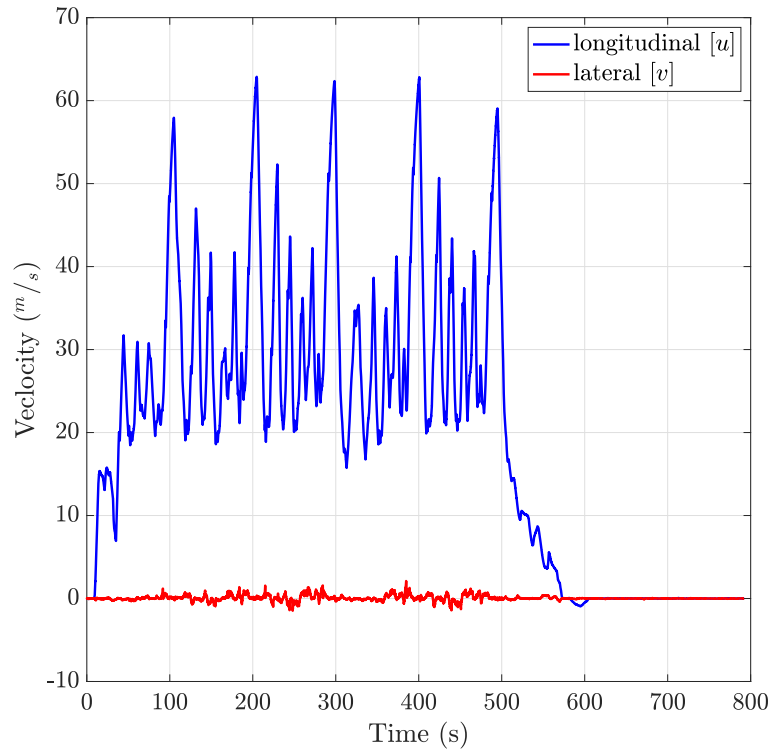


Figure 3.1: lateral and longitudinal velocity vs time

From Figure 3.1, the magnitude of the longitudinal velocity u is higher than the lateral

velocity v . This matches what was expected as the vehicle mainly moves longitudinally and only laterally while slipping. v also appears to have larger variations.

Q. Evaluate the longitudinal speed using the Hall-effect wheel speed sensors and compare the data with the INS data

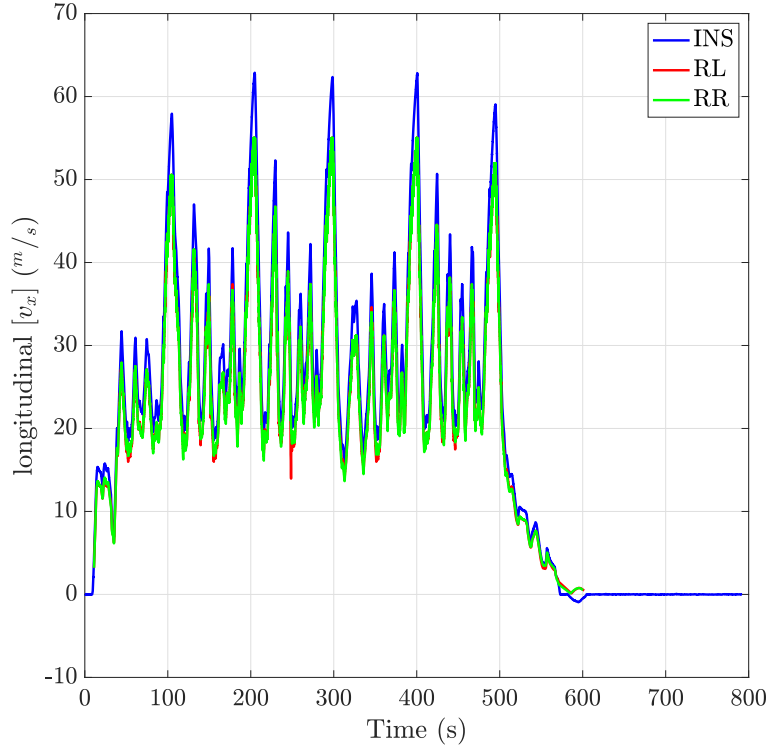


Figure 3.2: INS vs RL/RR hall effect sensors v_x

The longitudinal speed for the vehicle was calculated using the hall effect sensor data. Only the rear wheels [left and right] were used for the calculation. That is because they do not have a torque applied on them and they are “free rolling”. Every change in voltage [tick] means a full revolution of the tire. The time difference between 2 ticks was calculated [\bar{T}] and used in equation 3.1 to estimate the longitudinal speed [Where c is the wheel circumference]:

$$v_{wheel} = \frac{c}{\bar{T}} \quad (3.1)$$

The INS velocity is sometimes bigger than the hall effect calculated speeds, especially during braking [partial wheel lock]. There is no obvious difference between them during acceleration, which mean no significant wheel spin has been detected (Figure 3.2).

Q. Evaluate the lateral acceleration using the relation with the Ω and u .

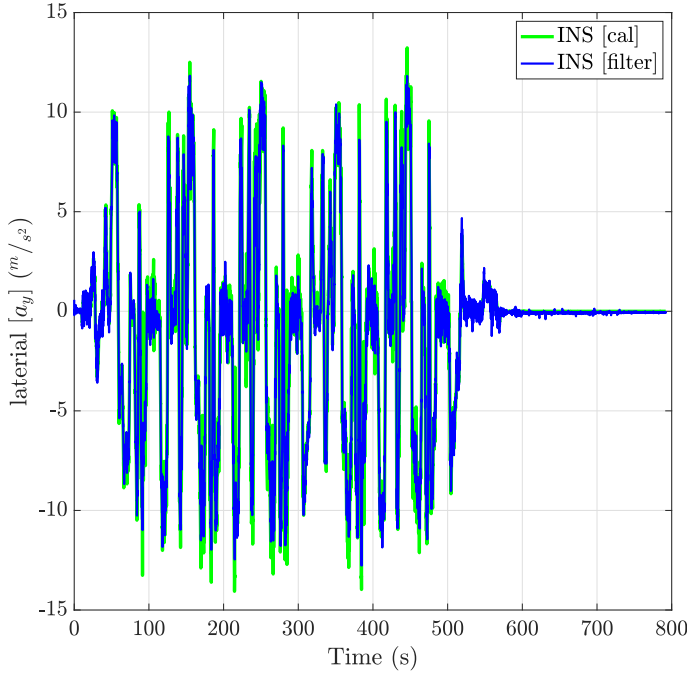


Figure 3.3: filtered INS vs calculated a_y

The lateral acceleration was calculated by multiplying the yaw rate by the longitudinal velocity, and is shown in Figure 3.3. This means that the following assumptions were true:

1. The vehicle has stayed in steady state where \dot{v} is small and $a_y \simeq \Omega u$
2. the road banking was negligible

Q. Comparing the longitudinal acceleration measured by INS with the one obtained by derivation of the longitudinal speed measured from the Hall sensors.

The derived acceleration a_x [shown in Figure 3.4] is quite noisier than the one provided by INS. The derived acceleration was filtered using a moving mean. This resulted in a far better matching acceleration compared to the INS data.

Q. Evaluate the side slip angle.

In Figure 3.5, the side slip angle β was calculated using the equation $\beta = \arctan(v/u)$. It appears that both the calculated and the INS provided β are similar, meaning that the INS is using the same formula. When $u \simeq 0$, the calculation becomes very noisy. The INS might be employing sensor fusion to suppress that noise. $\beta \in [-3, 5]$ which is considered small.

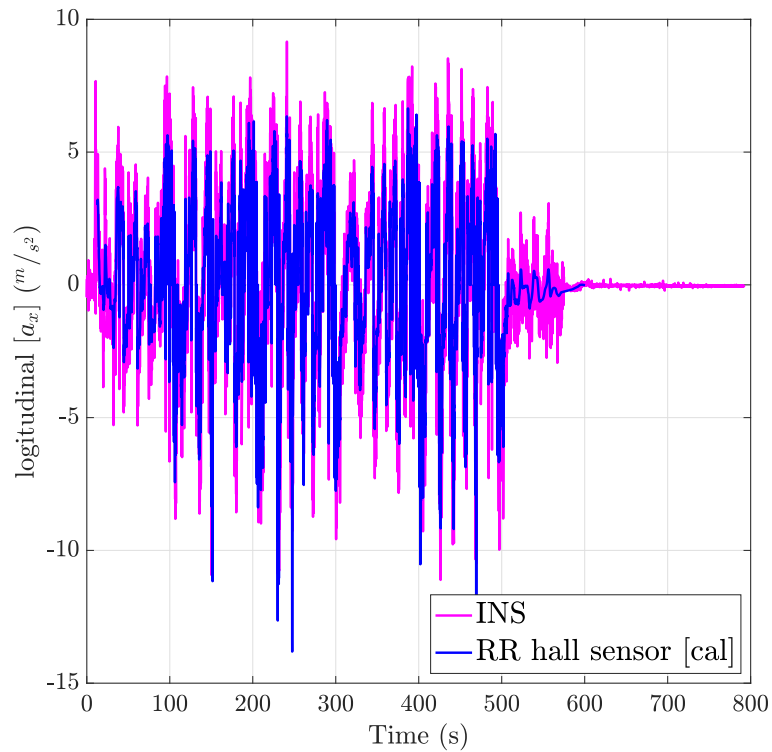


Figure 3.4: INS vs RR wheel hall effect derived a_x

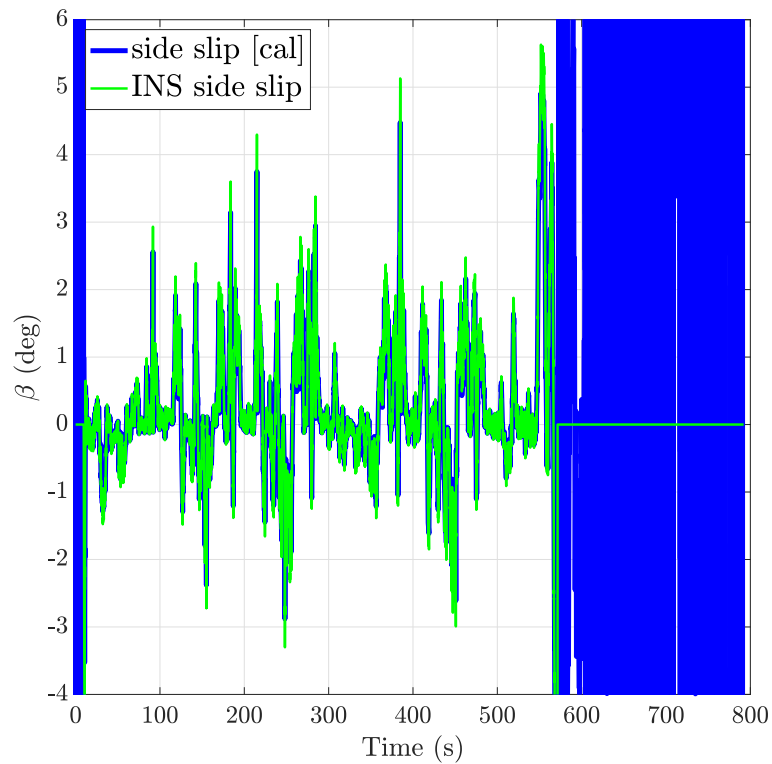


Figure 3.5: INS vs calculated side slip angle

Assignment 4

Vehicle Model Exercises

4.1 Exercise 1 - Vehicle Model Implementation

Q. For each maneuver, plot and comment the main results that you obtain, particularly focusing on tire forces and moments ($\{F_x, F_y, F_z, M_z\}$) and tire slips ($\{\kappa, \alpha\}$).

1. initial conditions: $u_0 = 30 \text{ km/h}$
 simulation timing: $T_s = 0.001 \text{ s}$, $T_f = 20 \text{ s}$
 requested pedal: req_pedal = 1
 requested steering wheel angle: req_steer = 0 deg.

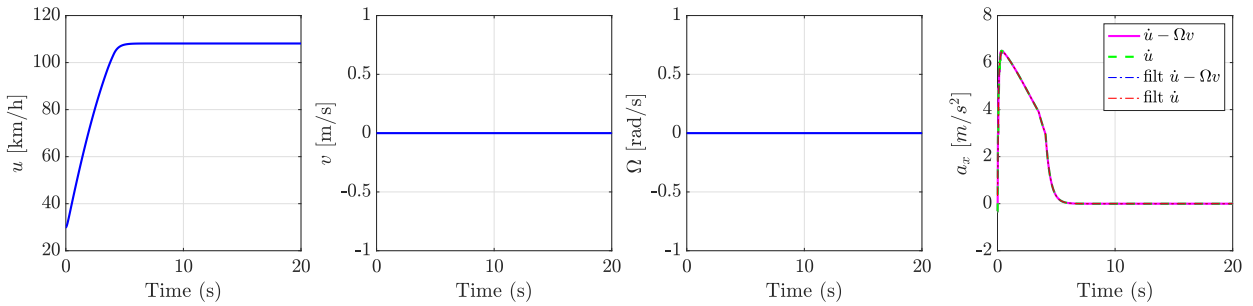


Figure 4.1: vehicle motion graphs [maneuver #1]

Figure 4.1 shows the motion graphs of the first maneuver. The vehicle starts from 30 km/h, with no steering input and full throttle. The velocity increased until it reached full speed of 108 km/h within 5 seconds. All upcoming graphs are influenced by the acceleration profile.

Assignment 4 – Vehicle Model Exercises

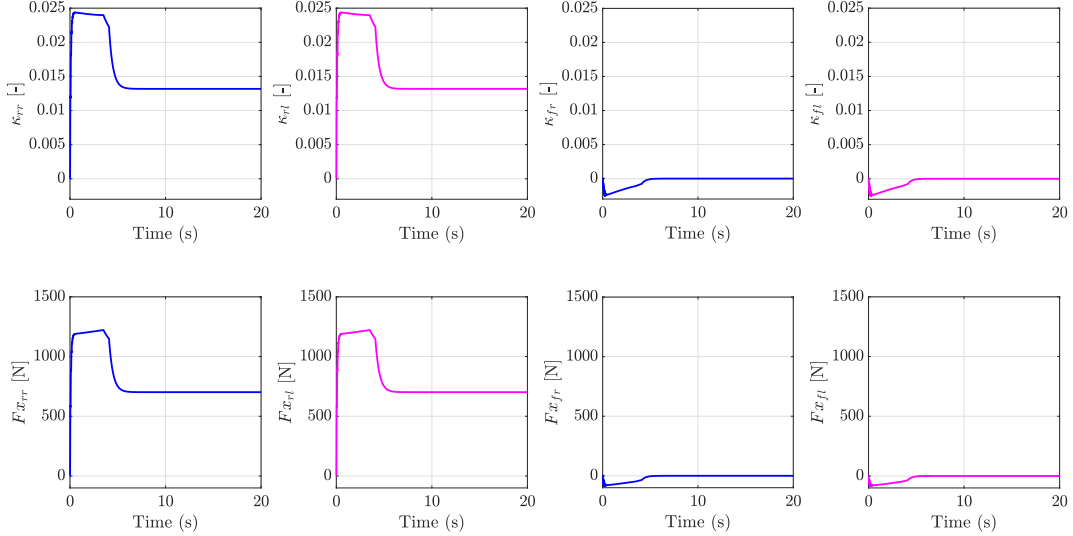


Figure 4.2: longitudinal slip κ and longitudinal forces F_x [maneuver #1]

The graphs in Figure 4.2 shows no difference between both right tires [and similarly the left tires] as the vehicle was moving straight without steering input. However, both rear tires show much higher κ and F_y . This was expected as the vehicle is rear-wheel drive and torque applied from the motors would increase both the slip and force experienced by the rear tires.

During the vehicle's acceleration to maximum speed [between 0 and 5 seconds], all tires showed higher slip and force. Once maximum speed is reached [acceleration is zero], the slips and forces decrease across all tires. The front tires go to zero, while the rears do not, as the motors must still keep applying [decreased] torque to keep the vehicle at speed.

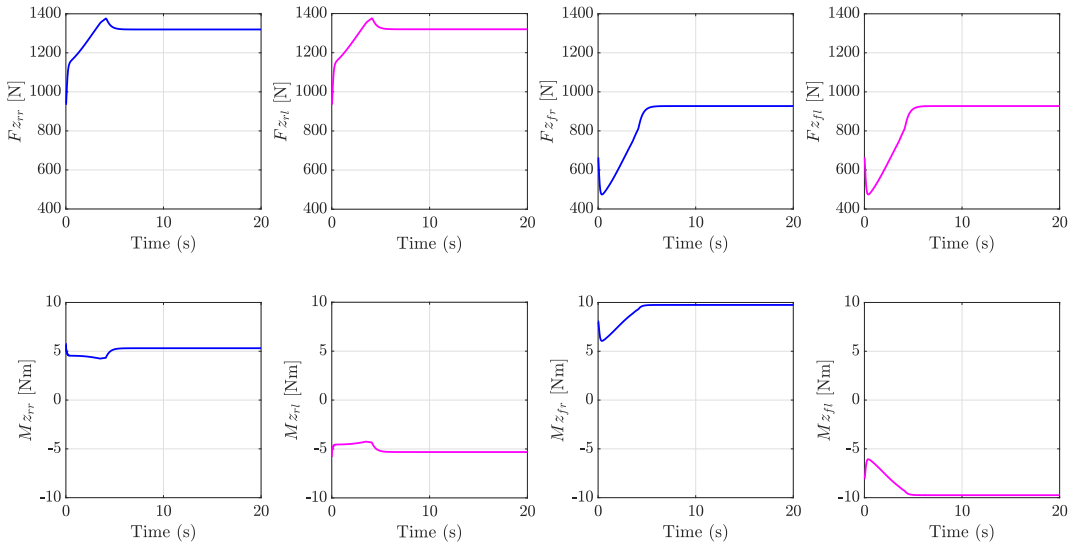


Figure 4.3: Vertical forces F_z and self aligning torque M_z [maneuver #1]

Assignment 4 – Vehicle Model Exercises

The aerodynamics load F_A increases as speed increases. As shown in Figure 4.3, the vertical force F_z increases across all tires because it relies on F_A . The vertical loads are calculated using Equation 4.1:

$$\begin{aligned} F_{zr} &= mg \frac{L_f}{L} + F_{Azr} + F_x \frac{h_G}{L} - \frac{I_{yz}}{L} \dot{\Omega} \\ F_{zf} &= mg \frac{L_r}{L} + F_{Azf} + F_x \frac{h_G}{L} - \frac{I_{yz}}{L} \dot{\Omega} \end{aligned} \quad (4.1)$$

They later reach steady state once the car stops accelerating. the rear tires show a peak in F_z due to the drop in acceleration a_y towards nearing maximum speed, which decreased the lateral load transfer on the rear tires.

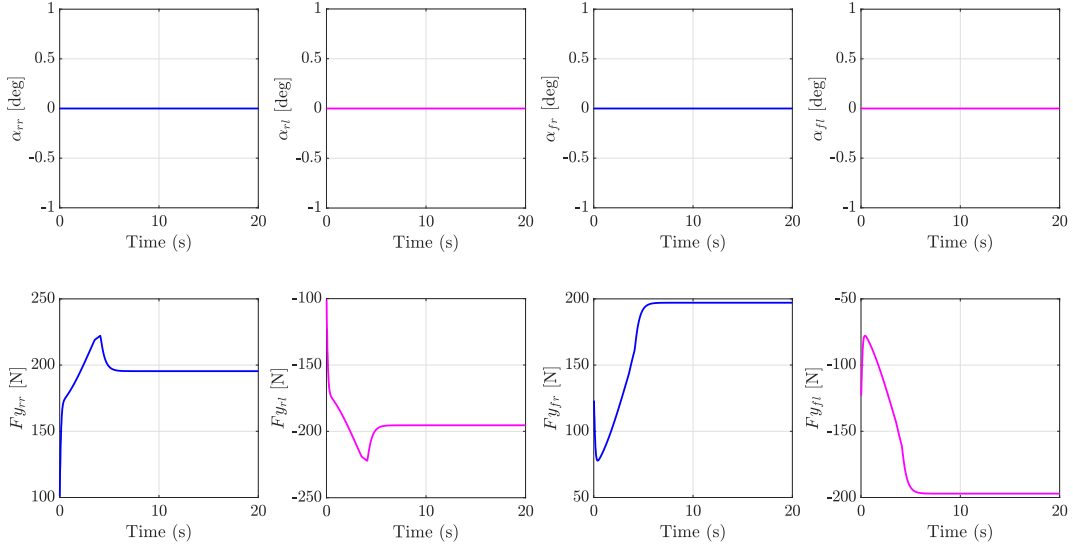


Figure 4.4: side slip angle α and lateral forces F_y [maneuver #1]

As previously mentioned, the vehicle has no steering input, which is why the side slip angle α for all tires are zero [Figure 4.4]. Furthermore, the magnitude of the lateral forces on the right tires are equal [and similarly the left tires]. The right tires' lateral forces are opposite in direction compared to the left tires and equal in magnitude, thus making them cancel out keeping the vehicle moving straight. F_y is smaller than F_x for all the tires. The self aligning torque M_z profiles previously shown in Figure 4.3 resemble the lateral forces profiles for each tire as they are trying to counter their effect on the steering.

During acceleration, the lateral forces F_y across all tires increase because the vertical forces F_z increased. The lateral forces rely on the vertical forces in the pacejka calculations, which is why both the F_y and F_z profiles match for front and rear tires.

2. initial conditions: $u_0 = 100 \text{ km/h}$
 simulation timing: $T_s = 0.001 \text{ s}$, $T_f = 1.5 \text{ s}$
 requested pedal: req_pedal = -1
 requested steering wheel angle: req_steer = 0 deg.

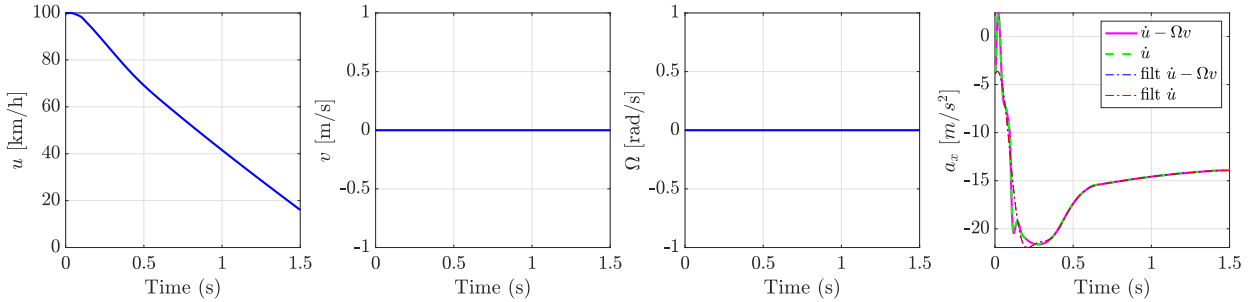


Figure 4.5: vehicle motion graphs [maneuver #2]

Figure 4.5 shows the motion graphs of the second maneuver. The vehicle starts from 100 km/h, with no steering input and applying full brakes. The velocity dropped to 16 km/h within the specified 1.5 seconds. The deceleration shows a decrease after 0.27 seconds as the rear tires start slipping and going into a full wheel lock as shown in Figure 4.6.

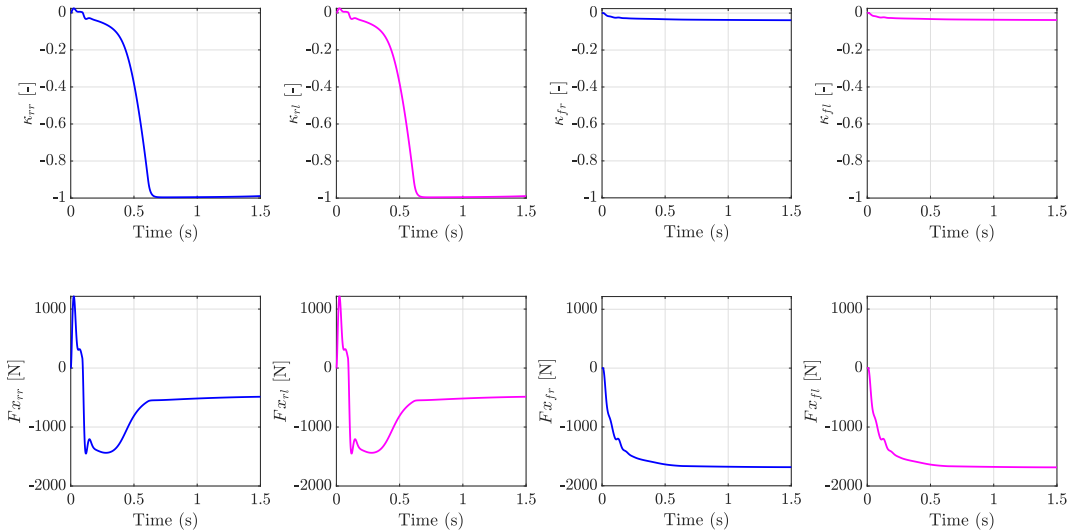


Figure 4.6: longitudinal slip κ and longitudinal forces F_x [maneuver #2]

This maneuver also doesn't have steering input, which is why the graphs in Figure 4.6 show no difference between both right and left tires. The longitudinal forces F_x for all tires increase in the opposite direction because the vehicle is decelerating. The longitudinal slip κ for the rear tires go to -1, which means both tires went into wheel lock. F_x decreases once wheel lock starts to occur causing lower efficiency in braking and the deceleration rate decreases.

Assignment 4 – Vehicle Model Exercises

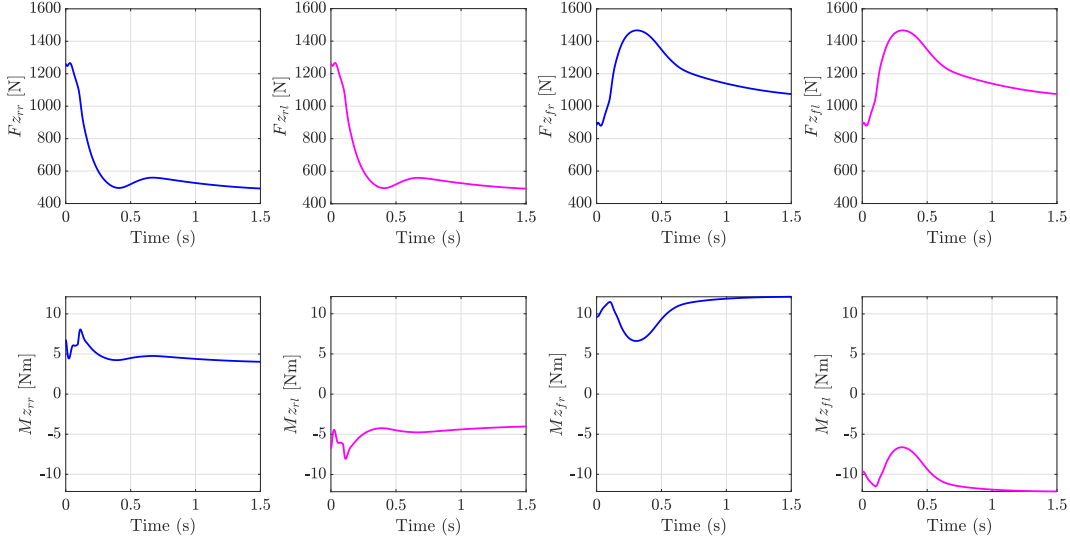


Figure 4.7: Vertical forces F_z and self aligning torque M_z [maneuver #2]

Figure 4.7 shows the vertical force F_z has decreased in the rear tires while increasing in the front. This is attributed to the longitudinal load transfer to the front because of the braking. The F_z forces on all tires showed a peak around 0.27 seconds due to the rear wheels locking.

No steering input means no side slip angle α for all tires [Figure 4.8]. And similar to maneuver #1, the right tires' lateral forces are opposite in direction compared to the left tires and equal in magnitude. The self aligning torque M_z profiles in Figure 4.7 for each tire are trying to counter the F_y 's effect on the steering. F_y showed the same trend as F_z , increasing in the front while decreasing in the rear tires.

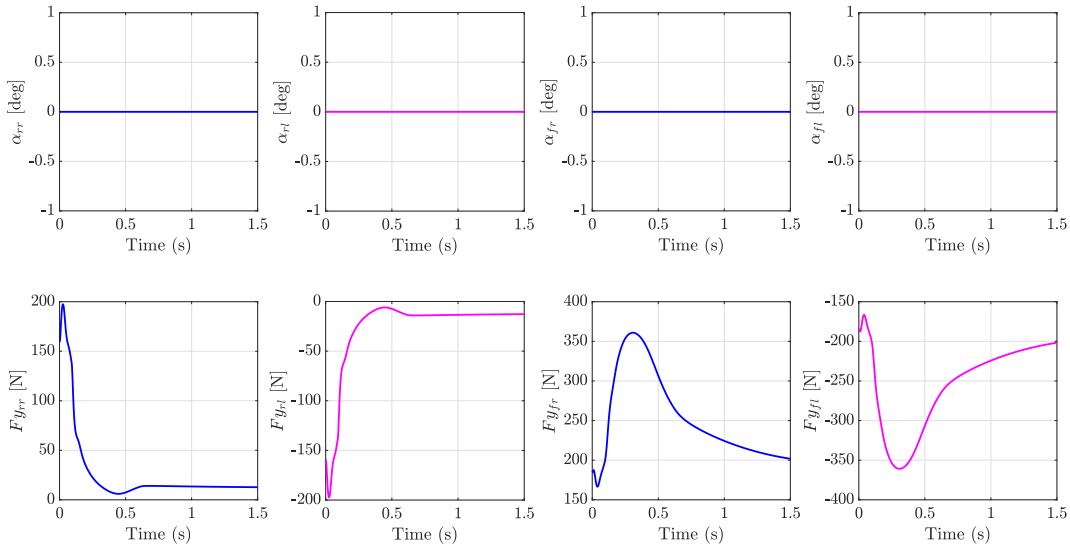


Figure 4.8: side slip angle α and lateral forces F_y [maneuver #2]

3. initial conditions: $u_0 = 50 \text{ km/h}$
simulation timing: $T_s = 0.001 \text{ s}$, $T_f = 1.5 \text{ s}$
requested pedal: req_pedal = 0.5
requested steering wheel angle: req_steer = 20 deg.

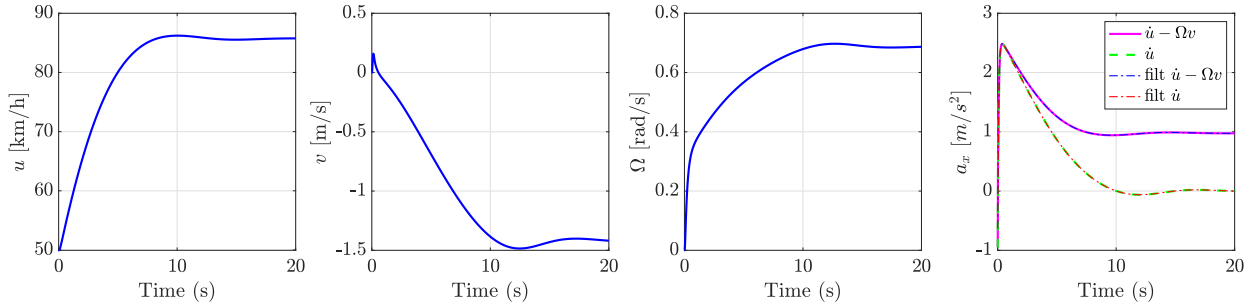


Figure 4.9: vehicle motion graphs [maneuver #3]

Figure 4.9 shows the motion graphs of the third maneuver. The longitudinal speed u keeps increasing until it reaches full saturation for half throttle. The lateral speed v shows the same profile as u . v is negative indicating the vehicle is turning left. The yaw rate Ω follows the same pattern, increasing during acceleration, and constant once acceleration is zero.

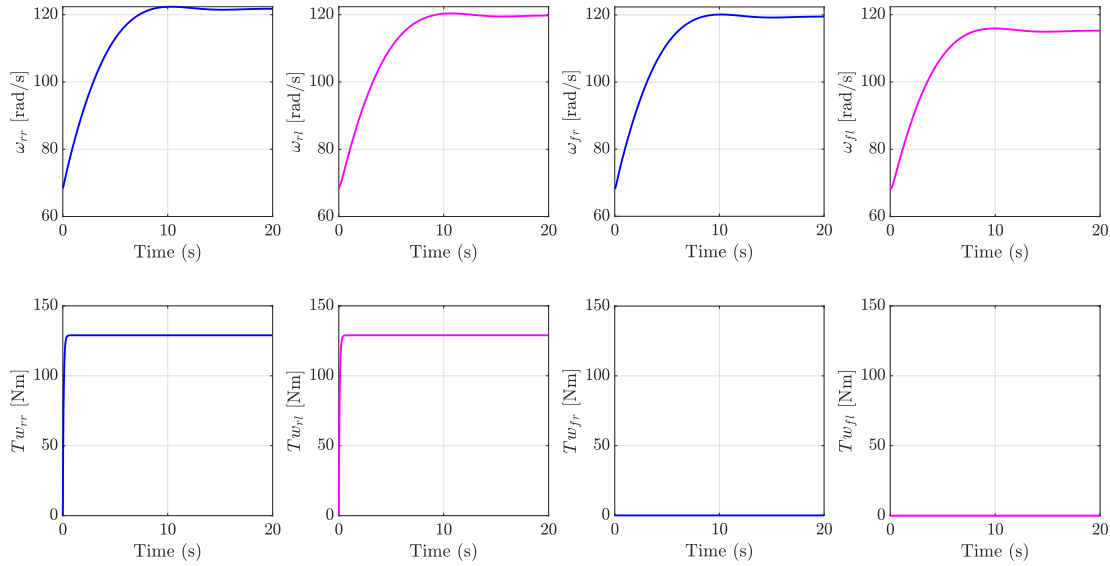


Figure 4.10: Wheel rates ω and Torques T_w [maneuver #3]

The angular velocity ω are different for different for each wheel as the outer [right] tires would need to rotate faster than the inner [left] tires [Figure 4.10]. The torque experienced by the rear tires are equal to each other, while the front ones are zero.

Assignment 4 – Vehicle Model Exercises

The longitudinal slip κ relies on ω for each wheel and can be calculated using Equation 4.2:

$$\kappa_{ij} = \frac{\omega_{ij} R_{ij} - v_{cxij}}{v_{cxij}} \quad i \in \{f, r\} \quad j \in \{r, l\} \quad (4.2)$$

Figure 4.11 shows κ and F_x . As there was no torque on the front tires, κ and F_x on the front tires were small. κ for the rear tires are different because they are rotating at different speeds. However, both rear tires still experienced the same F_x .

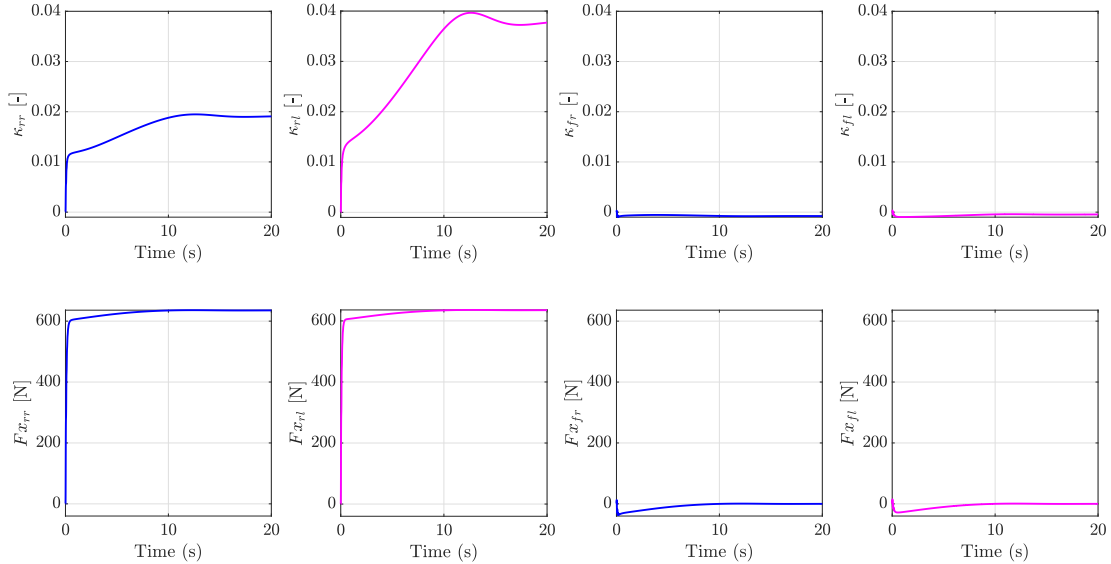


Figure 4.11: longitudinal slip κ and longitudinal forces F_x [maneuver #3]

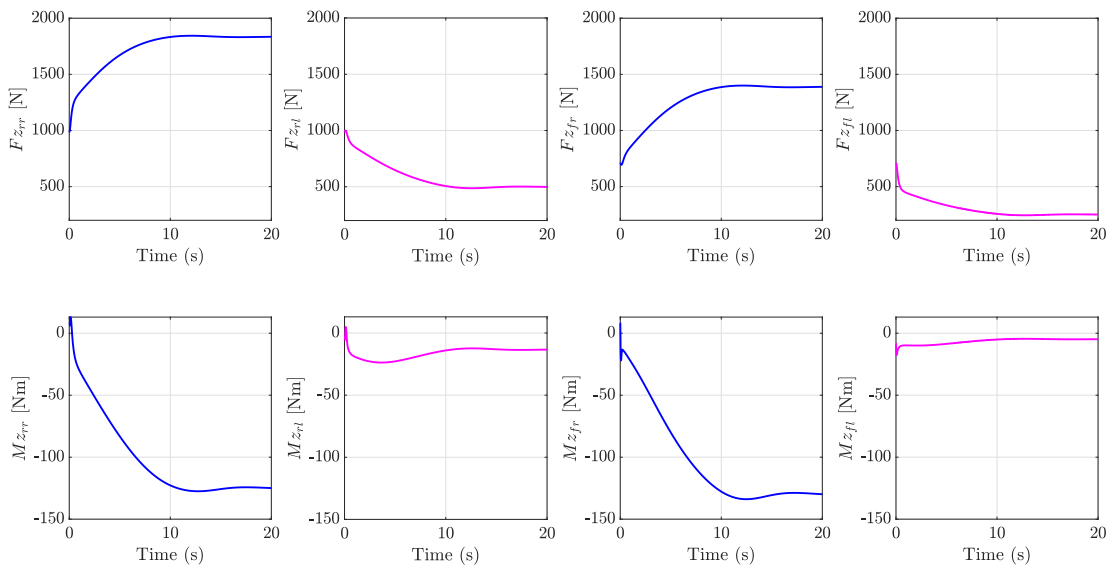


Figure 4.12: Vertical forces F_z and self aligning torque M_z [maneuver #3]

Assignment 4 – Vehicle Model Exercises

Figure 4.12 shows the vertical forces F_z for the right [outer] tires increasing then becoming constant when acceleration becomes zero. The left [inner] tires experienced the opposite because of the lateral load transfer to the right side of the vehicle due to the left turn.

The lateral side slip α for all tires are calculated using Equation 4.3:

$$\alpha_{ij} = -\arctan\left(\frac{vc_{yij}}{vc_{xij}}\right) \quad i \in \{f, r\} \quad j \in \{r, l\} \quad (4.3)$$

α appears to be consistent across the four tires as shown in Figure 4.13. However, the rear tires are slightly higher due to the torque applied by the motors.

The right side tires have higher lateral forces F_y compared to the right. This is because F_y relies on F_z , as the lateral load transferred to the right side during the left turn maneuver. Both α and F_y become constant once the acceleration is equal to zero. The self aligning torque M_z profiles in Figure 4.12 for each tire are trying to counter the F_y 's effect on the steering.

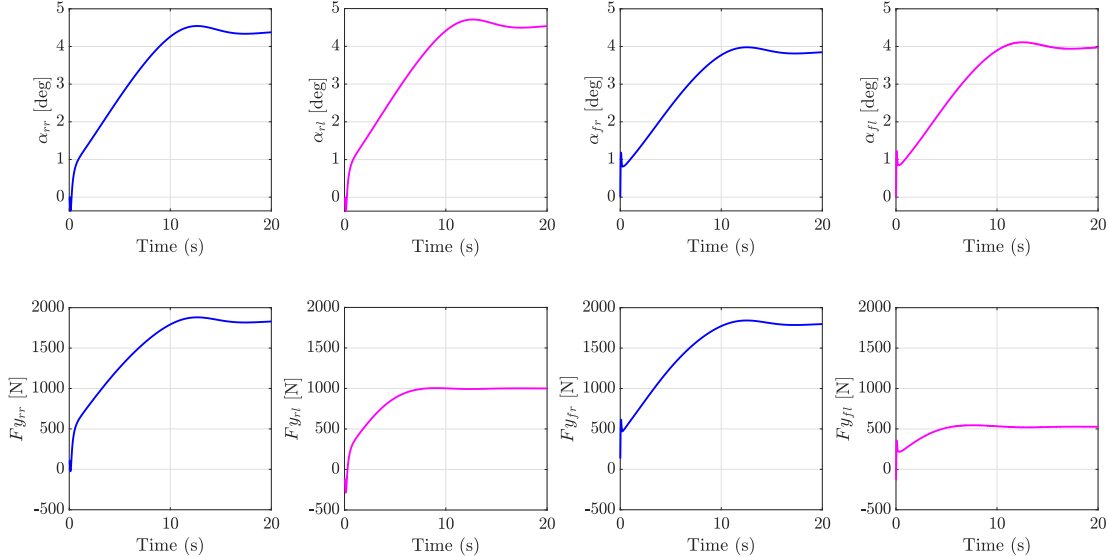


Figure 4.13: side slip angle α and lateral forces F_y [maneuver #3]

Assignment 5

Handling Identification

5.1 Exercise 1 - Sine Steer Maneuvers

Q. Perform a set of sine steer maneuvers, with steering wheel angle $\delta_D = \delta_{D0} \sin(2\pi ft)$. Use $\delta_{D0} = 5^\circ$, and repeat the test at 3 different $u = \{50, 80, 100\}$ km/h.

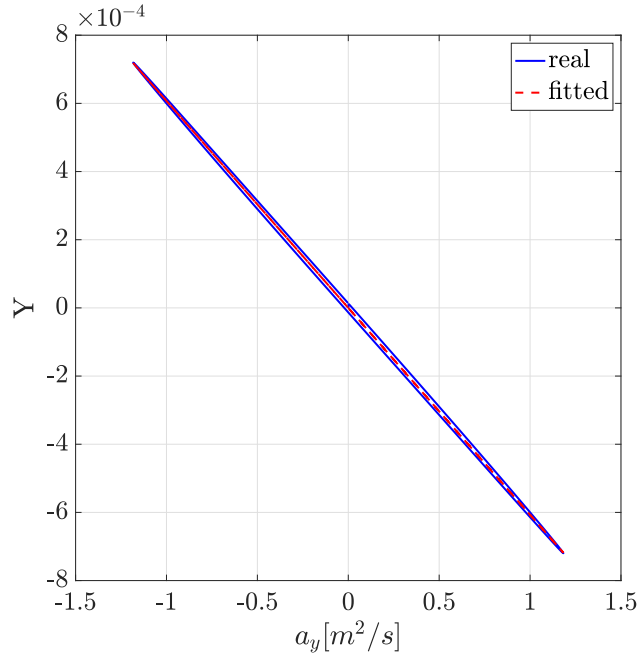


Figure 5.1: Fitted handling diagram result [$\delta_{D0} = 5^\circ$, $u = 50$ km/h]

Figure 5.1 shows the handling diagram result of a sine steering maneuver that uses a desired steering angle $\delta_D = \delta_{D0} \sin(2\pi ft)$ at speed 50 km/h. The frequency f in the equation is

Assignment 5 – Handling Identification

the number of complete cycles that happen every second. We must perform changes to our system very slowly in order to preserve steady state conditions. The frequency used was 0.001 s^{-1} and the simulation time was 1000 seconds. The Y refers to the handling behaviour of the vehicle and is calculated using Equation 5.1:

$$Y = \delta - \frac{\Omega}{u} L \quad (5.1)$$

The handling curve obtained at 50 km/h has a negative slope and appears to be linear. The data can be fitted with a first degree polynomial [$f(x) = ax + b$] as shown in Figure 5.1.

The negative slope indicates that the vehicle exhibits an over-steering behaviour. Over-steering occurs when the vehicle's rear wheels have higher lateral slip compared to the front [$\alpha_r > \alpha_f$]. This causes the rear wheels to have a larger radius of curvature than the front and the vehicle steers more than expected. If we want to keep the same radius of curvature in an over-steering condition, we must decrease the steering angle δ at higher velocities.

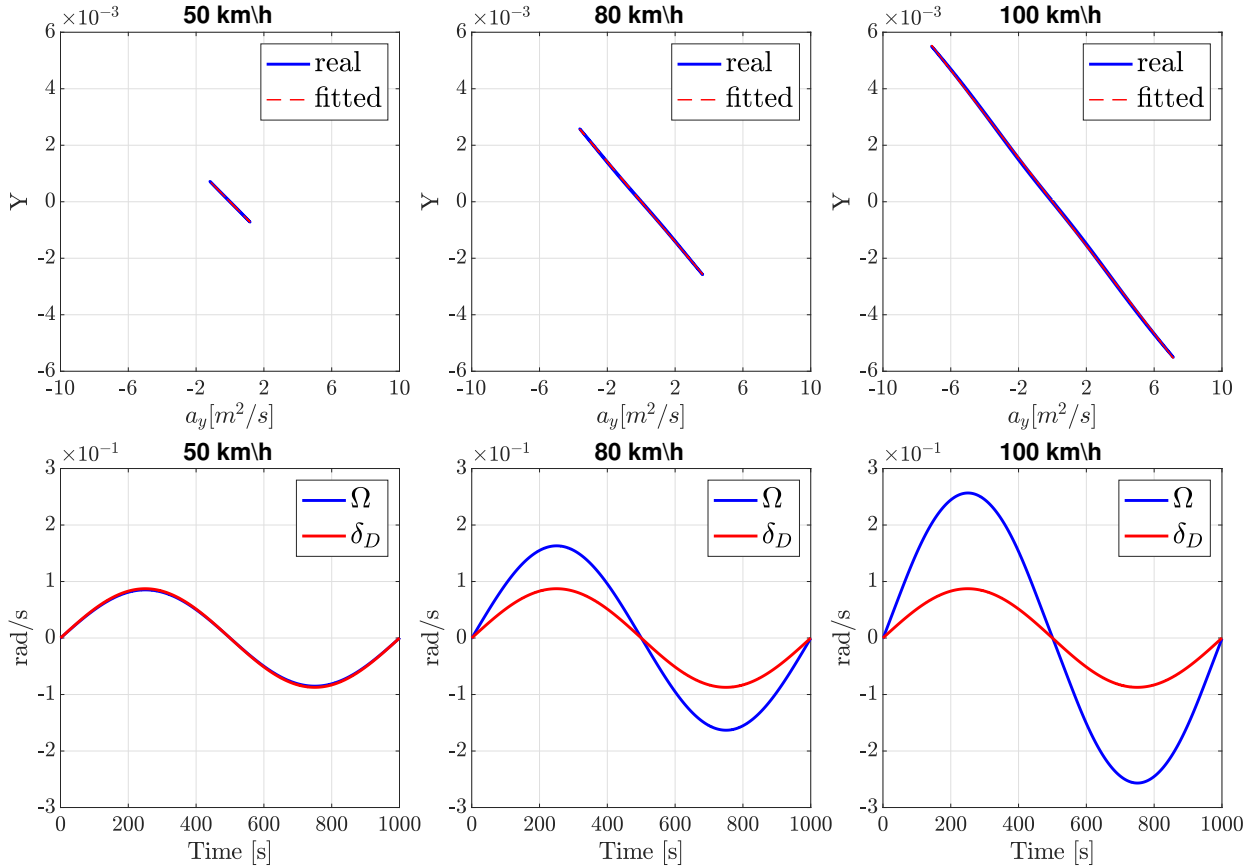


Figure 5.2: Handling diagram results at different speeds with same δ_D

Assignment 5 – Handling Identification

The slope of the line represents the under-steering gradient K_{us} , which describes the evolution of δ as a_y increases. K_{us} is positive if the vehicle is under-steering and negative when over-steering.

Increasing the speeds to 80 and 100 km/h resulted in an increase in the lateral acceleration a_y as shown in Figure 5.2. The vehicle nonetheless showed over-steering behaviour across all the simulated speeds. A comparison between the yaw-rate Ω and the desired steering angle δ_D shows that Ω keeps increasing with higher speeds even though δ_D is staying the same.

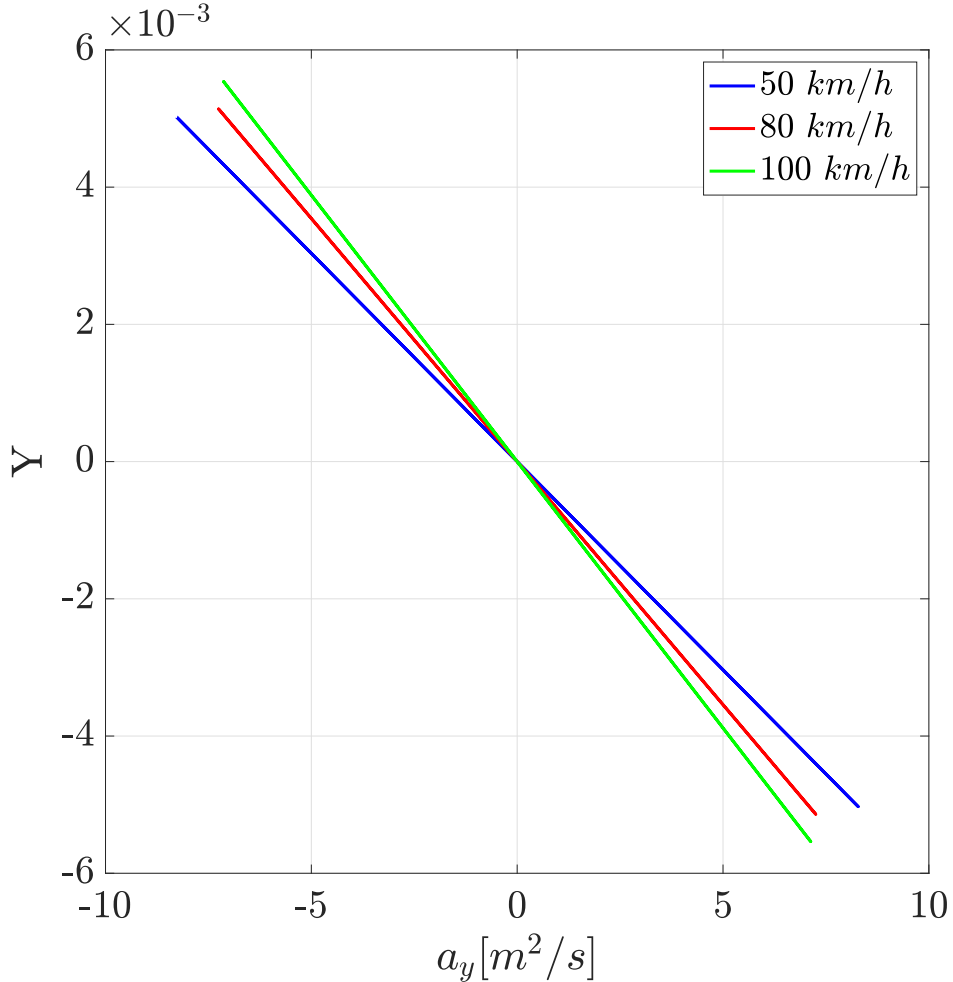


Figure 5.3: Fitted handling curves comparison with same δ_D

Superimposing the handling curves of the three simulated speeds in Figure 5.3 clearly shows that with higher speeds, the over-steering behavior increases [steeper negative slope]. That means δ will need to be decreased even further with higher speeds to keep the same curvature. Furthermore, the obtained curves pass through the origin. That means when there is no lateral acceleration a_y , the steering behaviour will be neutral.

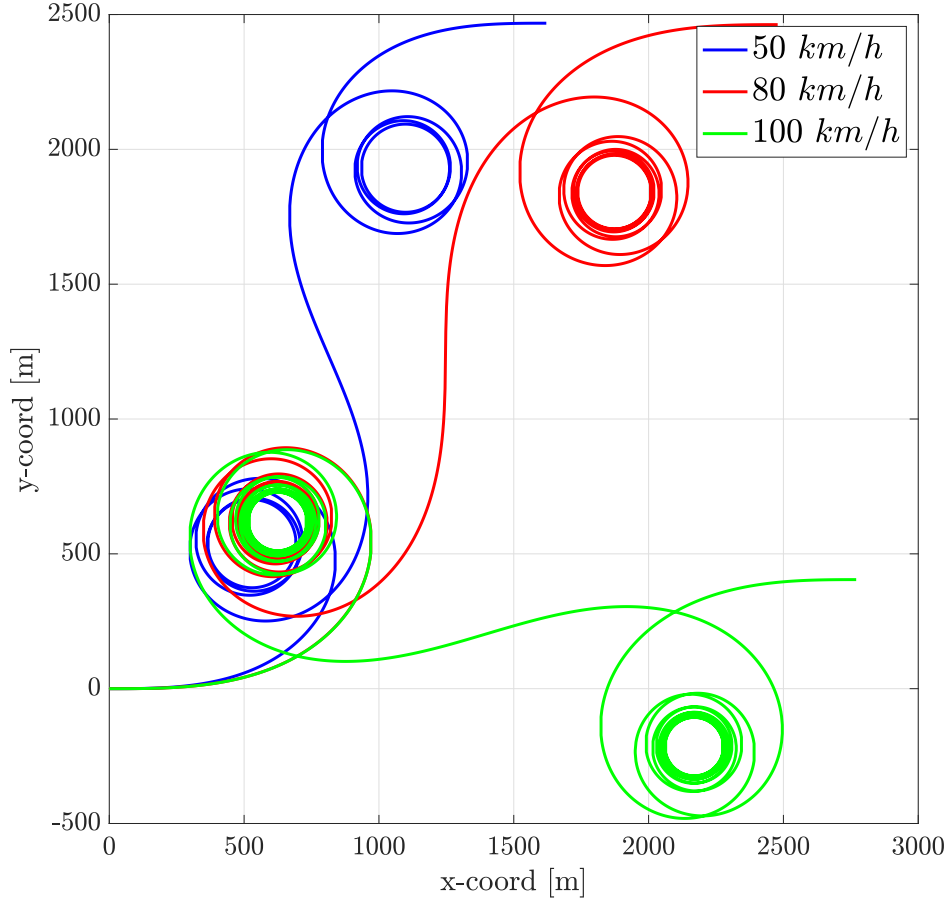


Figure 5.4: Vehicle paths for sine steer at different speeds with same δ_D

Plotting the path results of the three different speeds, as shown in Figure 5.4, confirms the over-steering behaviour. The radius of the curvature [the size of the circles] decreases with increasing velocities.

Q. carry out other 3 sine steer maneuvers, with these data:

1. $\delta_{D0} = 70^\circ$, $u = 50 \text{ km/h}$
2. $\delta_{D0} = 24^\circ$, $u = 80 \text{ km/h}$
3. $\delta_{D0} = 12^\circ$, $u = 100 \text{ km/h}$

Figure 5.5 shows the results of maintaining the vehicle's longitudinal velocity u at 50 km/h. A sinusoidal steering maneuver was applied with a large amplitude [70°] and a frequency f of 0.001 s^{-1} . This maneuver shows that the vehicle's handling behaviour changes when the lateral acceleration a_y increases above a certain threshold.

Assignment 5 – Handling Identification

The previous runs only had a maximum steering angle of 5° , which is considered small. With a much bigger maximum steering angle of 70° , the vehicle exhibits a linear over-steering behaviour while a_y is below $10 \text{ m}^2/\text{s}$. Once full saturation is reached, the slope of the curve becomes positive indicating that the behaviour has switched to under-steer.

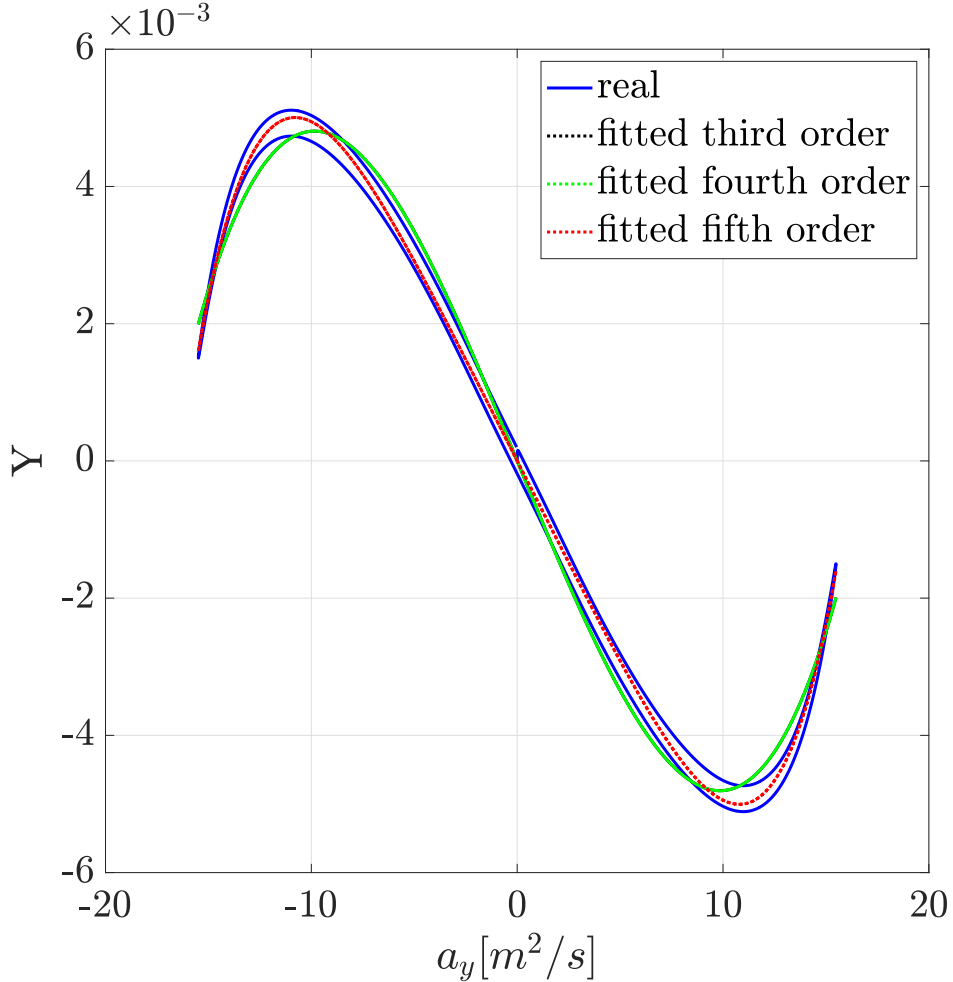


Figure 5.5: Fitted handling diagram result [$\delta_{D0} = 70^\circ$, $u = 50 \text{ km/h}$]

The curve can no longer be fitted with a first degree polynomial. Polynomial degrees from one to five were tested, and the lowest and best fitting ones are shown in Figure 5.5. It appears that a fifth order polynomial is the best approximation for such a curve.

Figures 5.6 and 5.7 show the results of the second and third runs. The effect of higher lateral acceleration a_y on the handling behaviour is not as prevalent in both runs, because the maximum steering angle was much smaller [12° and 24° compared to 70°]. The overall behaviour for the second and third runs stayed as over-steering across a_y . However, the curve is not linear. A third order polynomial was the best fitting for both runs.

Assignment 5 – Handling Identification

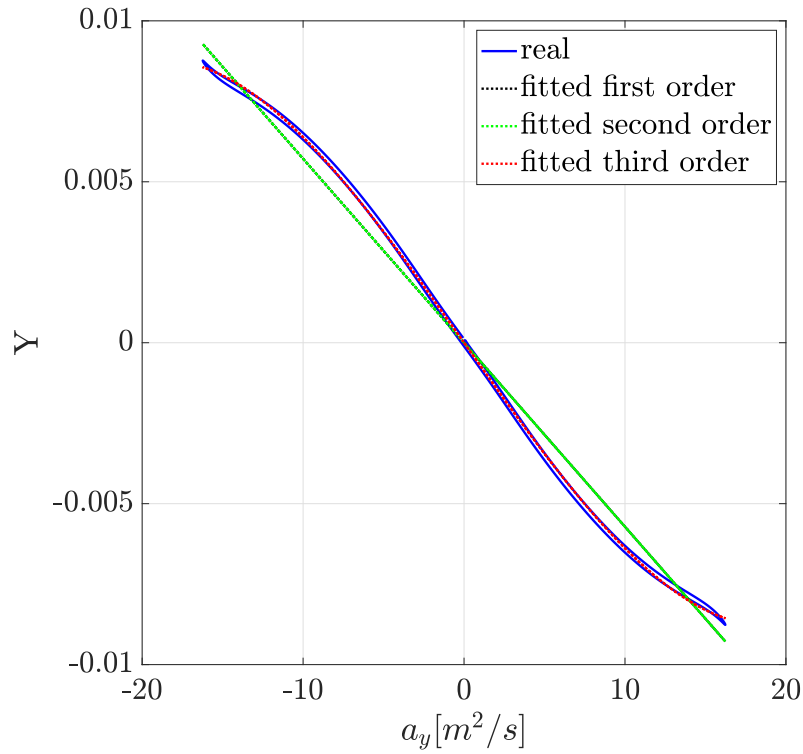


Figure 5.6: Fitted handling diagram result [$\delta_{D0} = 24^\circ$, $u = 80 \text{ km/h}$]

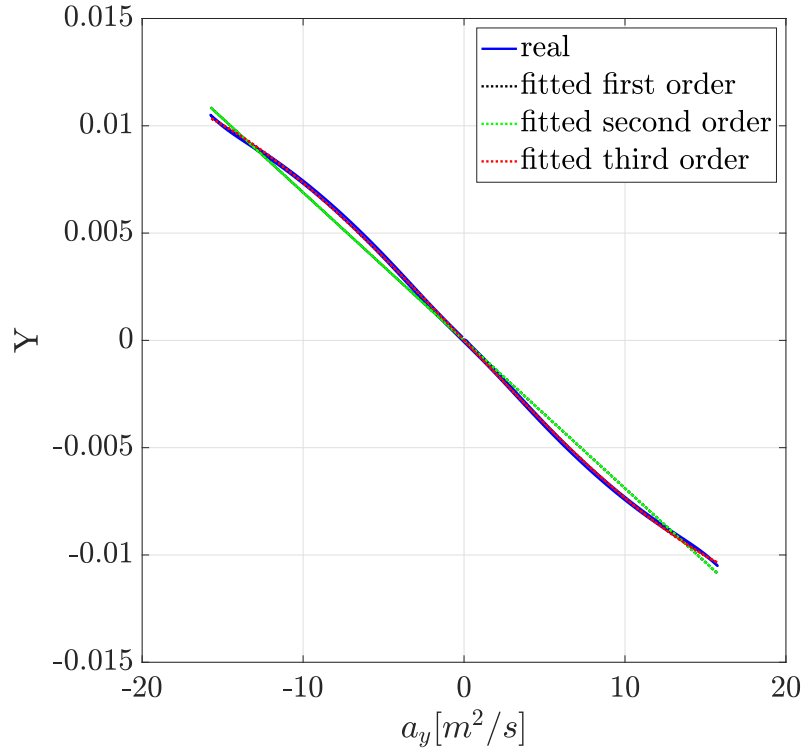


Figure 5.7: Fitted handling diagram result [$\delta_{D0} = 12^\circ$, $u = 100 \text{ km/h}$]

Coefficients of the polynomial fittings:

```
run# 1: [0.0013296, -1.6137e-07, 0.0003224, 3.9837e-07, -0.0066391, -1.9657e-07]
run# 2: [0.0010692, 6.2659e-08, -0.0082143, -9.0719e-08]
run# 3: [0.0007569, 7.6441e-08, -0.0089127, -8.4754e-08]
```

The results of all the coefficients for the fittings for the three runs are shown above. They are certainly not constant across the runs because they fit different curves. However, some are quite close, especially runs # 2 and 3. This could be attributed to the similarity in the linear sections of the three curves as shown in Figure 5.8.

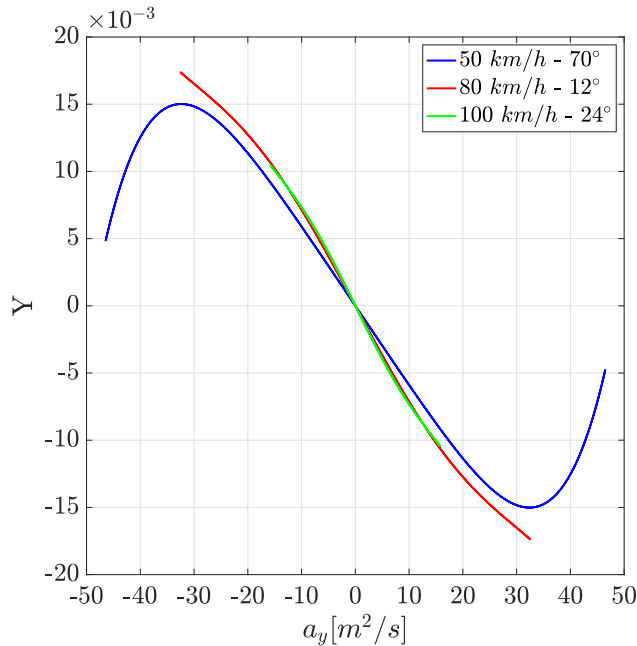


Figure 5.8: Fitted handling curves comparison with different δ_D

5.2 Exercise 2 - Constant Steer Maneuvers

Q. Carry out a constant steering maneuver, with these data:

1. $\delta_D = 10^\circ$, $u_0 = 20 \text{ km/h}$, $u_f = 40 \text{ km/h}$
2. $\delta_D = 24^\circ$, $u_0 = 50 \text{ km/h}$, $u_f = 80 \text{ km/h}$

The simulations were run for 1000 seconds. Figure 5.9 shows the motion graphs for maneuver #1 [only plotting the first 10 seconds]. The speed ramped up from 20 to 40 km/h within the first 2 seconds using the low level PID controller to manage the pedal.

Assignment 5 – Handling Identification

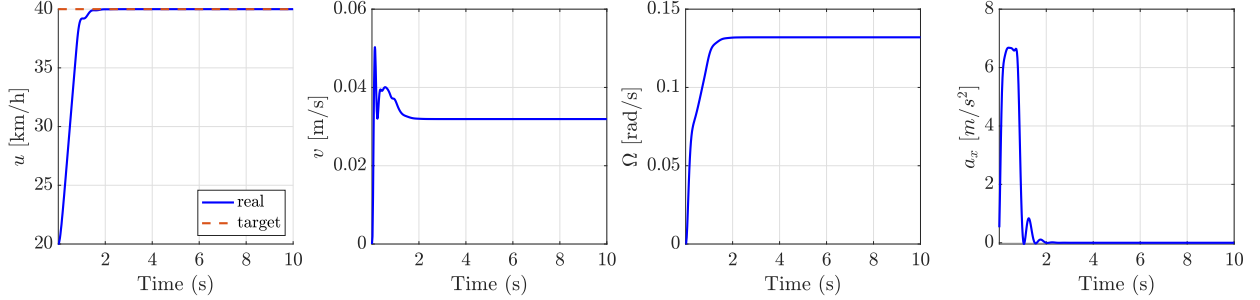


Figure 5.9: Vehicle motion graphs for constant steer maneuver #1

The vehicle must be in steady state conditions in order to plot the handling curve. The data was filtered by monitoring the change in u using Equation 5.2. The data used in plotting begins at the (steady state start index) till the end [Figure 5.10].

$$\text{steady state start index} = \text{find}(\text{diff}(u)) \geq 0.003m/s \quad (5.2)$$

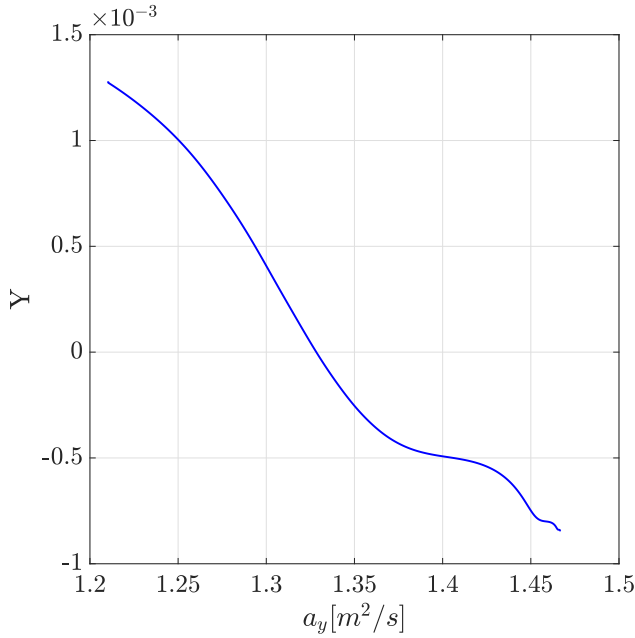


Figure 5.10: Filtered handling curve for constant steer maneuver #1

Even though the filtering has significantly improved the result of the graph, it still is not quite accurate enough. This might be due to the very low lateral acceleration a_y that the vehicle experienced during this maneuver. Nonetheless, the results still suggests that the vehicle has an over-steering behaviour.

Assignment 5 – Handling Identification

The path result of the maneuver plotted in Figure 5.11 shows that the curve was about 80 meters in radius and the vehicle ended almost at the start point. This indicates that the vehicle experienced a negligible amount of over-steer as it was not pushed hard enough to cause any front or rear tire slip.

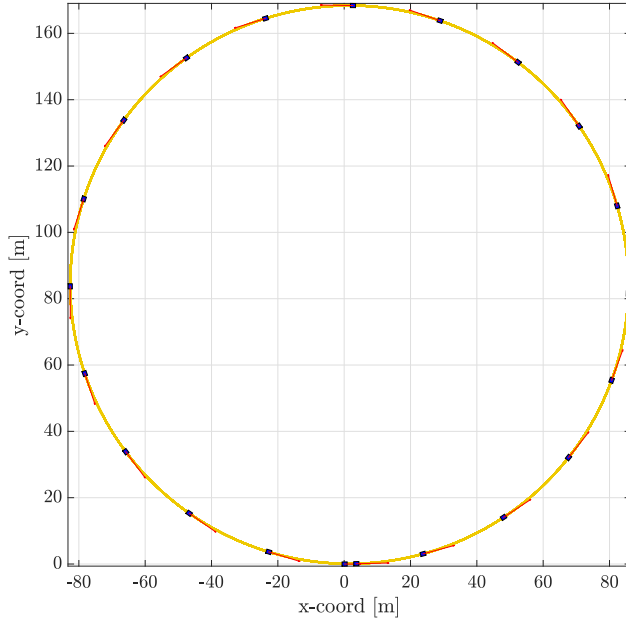


Figure 5.11: Path of the vehicle for constant steer maneuver #1

Similar to maneuver #1, Figure 5.12 shows the motion graphs for maneuver #2 [only plotting the first 10 seconds]. The speed ramped up from 40 to 80 km/h within the first 3 seconds using the low level PID controller to manage the pedal.

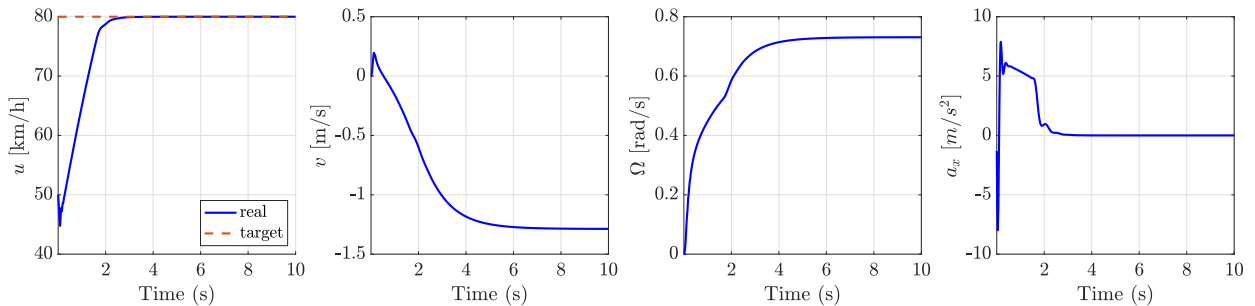


Figure 5.12: Vehicle motion graphs for constant steer maneuver #2

The filtered handling curve for maneuver #2 in Figure 5.13 is significantly better than the previous maneuver. this could be attributed to the much higher lateral acceleration a_y encountered. The curve is almost linear and has a negative slope, which agrees with all the previous maneuvers.

Assignment 5 – Handling Identification

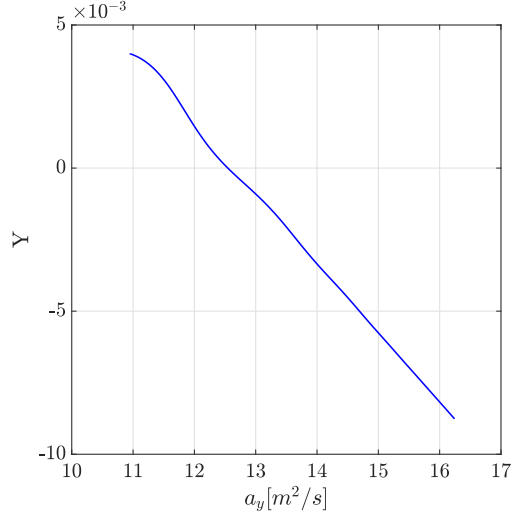


Figure 5.13: Filtered handling curve for constant steer maneuver #2

The radius of the path with the second maneuver plotted in Figure 5.14 has a much smaller radius [40 meters]. The vehicle has certainly experienced over-steer because the curvature decreased towards the end of the run.

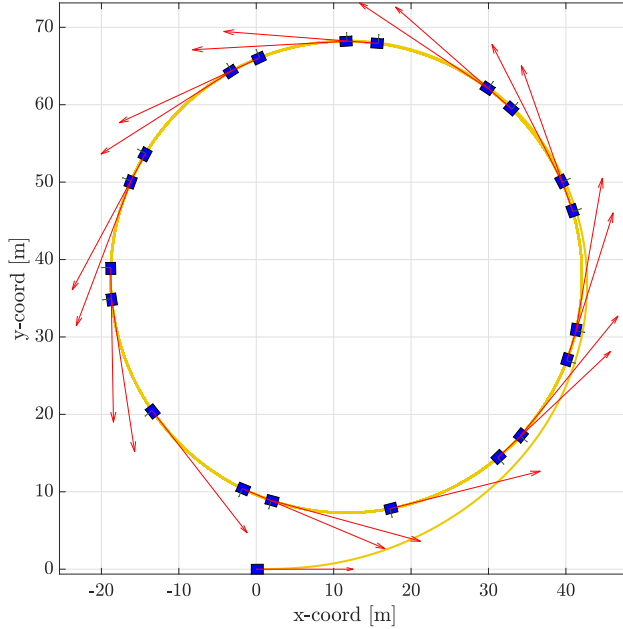


Figure 5.14: Path of the vehicle for constant steer maneuver #2

In conclusion, the steering gradient K_{us} is a function of multiple variables including (a_y, u, a_x) . To predict handling behaviour more accurately, the vehicle was tested from 20 to 100 km/h using the sine steer maneuver with a $\delta_D = 10^\circ$. The results are in Table 6.1 and Figure 5.15.

| u [km/h] | K_{us} |
|------------|-----------------------|
| 20 | -1.0×10^{-4} |
| 30 | -3.0×10^{-4} |
| 40 | -6.0×10^{-4} |
| 50 | -1.0×10^{-3} |
| 60 | -1.6×10^{-3} |
| 70 | -2.4×10^{-3} |
| 80 | -3.5×10^{-3} |
| 90 | -5.0×10^{-3} |
| 100 | -6.9×10^{-3} |

Table 5.1: Vehicle's K_{us} for tested speeds with sine steer [$\delta_D = 10^\circ$]

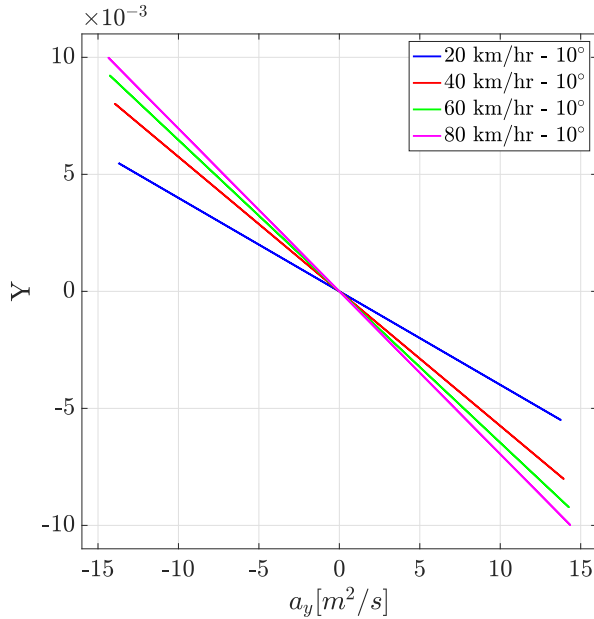


Figure 5.15: K_{us} results based on u with sine steer [$\delta_D = 10^\circ$]

| Sine steer | Constant Steer |
|--|--|
| More difficult to maintain steady state as the steering angle is changing constantly | Easier to maintain steady state considering that u is easier to regulate |
| Needs a robot to perform | Easily performed by a human driver |
| Perform left and right turns on the same run | Only perform either left or right turns per run |
| Requires a larger area to perform [going straight and steering left to right] | A smaller area is required to perform [going in circles] |

Table 5.2: Pros And Cons of the constant steer and sine steer tests

Assignment 6

Lateral Control

6.1 Exercise 1 - lateral control

Q. Optimize the clothoid-based lateral controller

The clothoid-based lateral controller uses Equation 6.1 to calculate the steering angle required to follow the clothid. The under-steering gradient K_{us} was calculated previously using the handling diagram shown in Table 5.1. These results were implemented as a variable that changes based on the vehicle's current speed.

$$\delta(s) = k(s)(L + K_{us}u^2) \quad (6.1)$$

To optimize the clothoid-based lateral controller look ahead variable, several tests were conducted using the following variables totalling 42 tests:

- $u = [10, 20, 30, 40, 50, 60, 70, 80]$ km/h
- look ahead = [5, 10, 15, 20, 25, 30]

The tracking error had to be calculated to compare the test results. That was done by using the “N-D nearest point search” function in Matlab, which returns indices of closest points in the desired path for each point on the real path. Then calculating the euclidean distance

Assignment 6 – Lateral Control

between each point in the real path and closest point on the desired path as tracking error. The results are shown in Figure 6.1 and Table 6.1 where LA is the look ahead value.

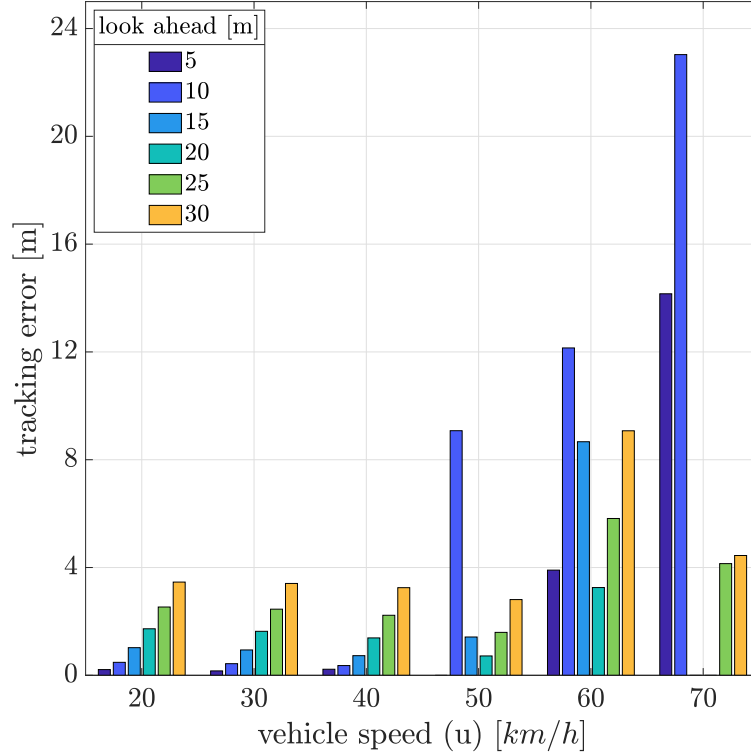


Figure 6.1: clothoid-based lateral controller at different u and look ahead

The tests checked if the vehicle was able to arrive at a designated target point chosen to be at [60,10]. If the vehicle reaches this point within a threshold of 5 meters, the test is considered a success.

| u [km/h] | LA = 5 | LA = 10 | LA = 15 | LA = 20 | LA = 25 | LA = 30 |
|------------|----------------------|----------------------|----------------------|----------------------|---------|---------|
| 20 | 2.1×10^{-1} | 4.8×10^{-1} | 1.0 | 1.7 | 2.5 | 3.5 |
| 30 | 1.6×10^{-1} | 4.3×10^{-1} | 9.4×10^{-1} | 1.6 | 2.5 | 3.4 |
| 40 | 2.3×10^{-1} | 3.6×10^{-1} | 7.3×10^{-1} | 1.4 | 2.2 | 3.3 |
| 50 | NA | 9.1 | 1.4 | 7.2×10^{-1} | 1.6 | 2.8 |
| 60 | NA | 1.2×10^1 | 8.7 | 3.3 | 5.8 | 9.1 |
| 70 | 1.4×10^1 | 2.3×10^1 | NA | NA | 4.1 | 4.4 |

Table 6.1: Tracking error results [clothoid-based lateral controller]

The red colored cells indicates the vehicle was not able to arrive at the designated target point. Green cells are the chosen look ahead values at each speed u .

Assignment 6 – Lateral Control

As expected, the larger the look ahead value, the larger the tracking error. Having a larger look ahead at 20 km/h could be beneficial if we are optimizing for traveled distance, and smoother turns [less jerk].

Figure 6.2 shows the vehicle actual path at each look ahead value for 20 km/h tests. A larger look ahead optimized the vehicles path to take a shorter route and take better turns. However, this caused the tracking error to increase, because we are not following the reference trajectory anymore.

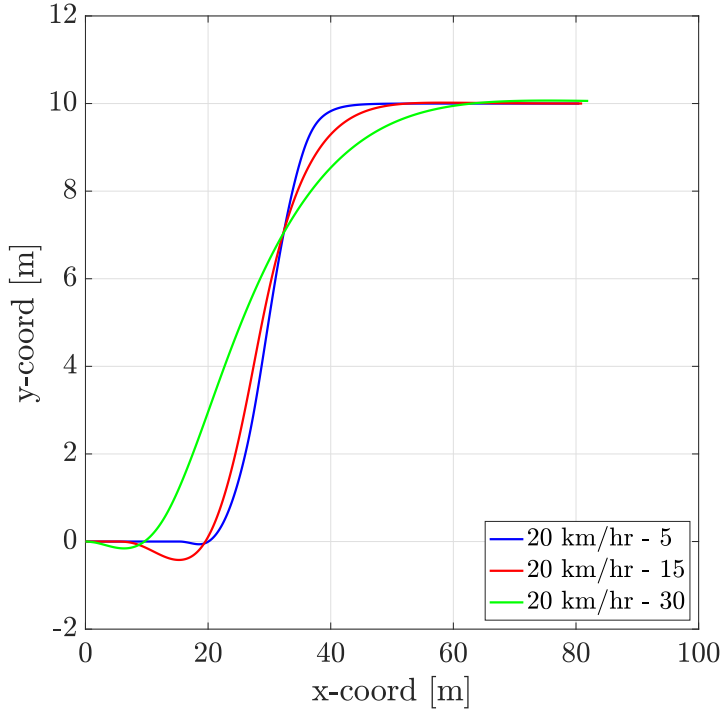


Figure 6.2: Real vehicle path with different look ahead values [$u = 20\text{km}/\text{h}$]

Up until 40 km/h, a lower look ahead value performed better for our metrics. With increasing u , the smaller look ahead values were simply not enough to control the vehicle properly. The controller needs to see far enough ahead to account for a curve earlier on. The faster the vehicle, the bigger the needed look ahead value.

Figure 6.3 shows the vehicle paths at 70 km/h at different values for the look ahead. The higher values are more stable but still considered outside the capabilities of the vehicle.

No values of look ahead was enough to stabilize the vehicle with any speed higher than 70 km/h. This might be attributed to the K_{us} values not being accurate enough at these speeds. The handling curves during these speeds were not linear anymore and a linear approximation

for them is not sufficient. It could be also attributed to the fact that the look ahead point is far ahead of the car that it has exceeded the reference trajectory and caused the vehicle to abruptly change the steering causing a loss in control.

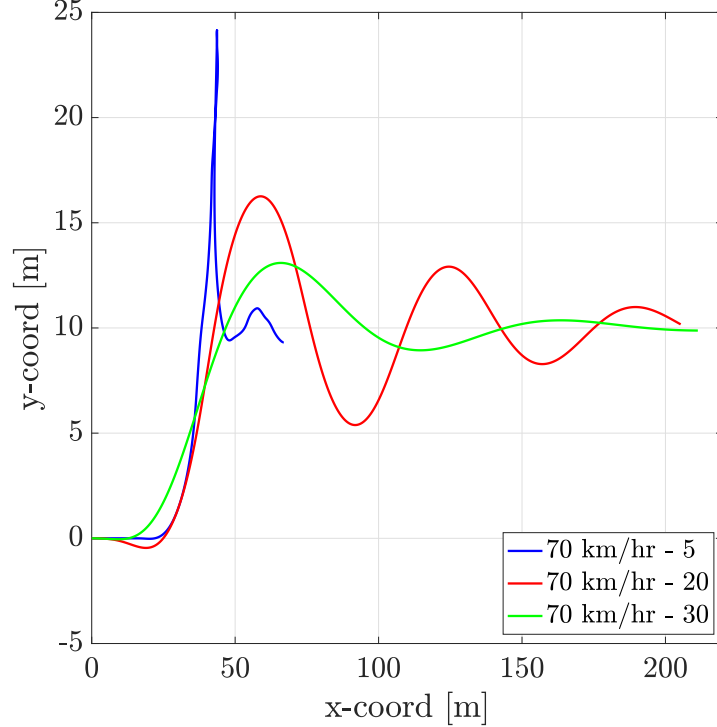


Figure 6.3: Real vehicle path with different look ahead values [$u = 70 \text{ km/h}$]

Q. Implement the pure pursuit controller and optimize the look ahead distance

Pure pursuit calculates the circular arc radius R between center of the vehicle's rear wheel P_V and the target point on the desired path P_D . Equation 6.2 is used to calculate R , where x_D and y_D are P_D expressed in the vehicle's frame. R is later used to calculate the required steering angle δ .

$$R = \frac{\sqrt{x_D^2 + y_D^2}}{2\sin(\lambda)} \quad \text{and} \quad \delta = \arctan(L/R) \quad (6.2)$$

To optimize the pure pursuit lateral controller look ahead variable, several tests were conducted using the following variables totalling 64 tests:

- $u = [20, 30, 40, 50, 60, 70, 80, 90, 100] \text{ km/h}$
- look ahead = [1, 2, 3, 4, 5, 10, 15, 20, 25, 30]

Assignment 6 – Lateral Control

The tracking error was calculated in the same manner as previous and some of the results are shown in Figure 6.4 and Table 6.2. The effect of the look ahead variable on the pure pursuit controller behaviour is similar to the clothoid-based controller. With higher speeds, larger look ahead values are required.

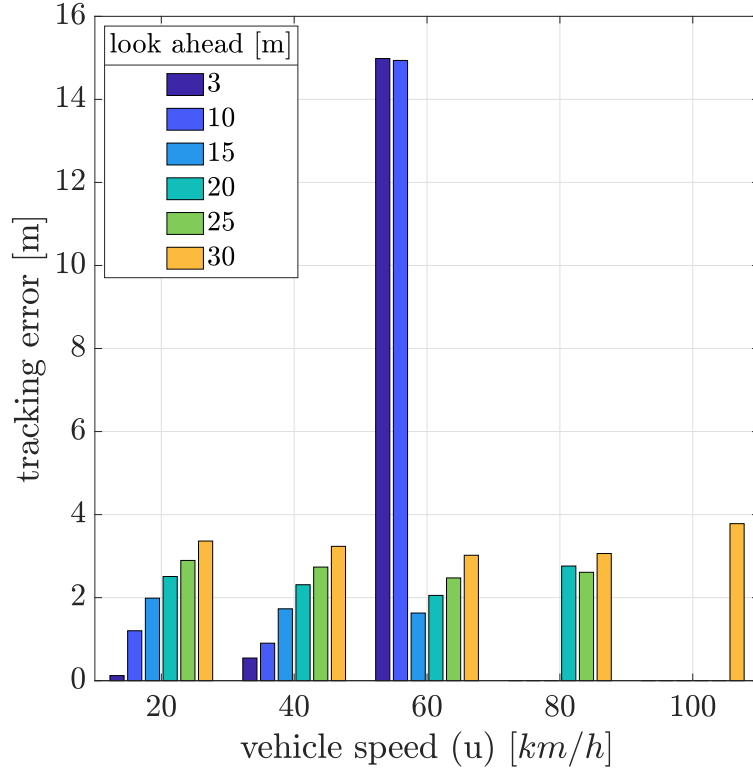


Figure 6.4: pure pursuit lateral controller at different u and look ahead

Overall, the pure pursuit controller performed well. Table 6.2 shows some of the tests conducted and their tracking error. The red colored cells indicate the vehicle was not able to arrive at the target point, while the green cells are the best performers for each speed u . A look-up table can now be used to choose the correct look ahead based on current speed.

| u [km/h] | LA = 3 | LA = 10 | LA = 15 | LA = 20 | LA = 25 | LA = 30 |
|------------|----------------------|----------------------|-------------------|---------|---------|---------|
| 20 | 1.2×10^{-1} | 1.2 | 2.0 | 2.5 | 2.9 | 3.4 |
| 40 | 5.5×10^{-1} | 9.0×10^{-1} | 1.7 | 2.3 | 2.7 | 3.2 |
| 60 | 1.5×10^1 | 1.5×10^1 | 1.2×10^1 | 2.1 | 2.5 | 3.0 |
| 80 | NA | NA | NA | 2.8 | 2.6 | 3.1 |
| 100 | NA | NA | NA | NA | NA | 3.8 |

Table 6.2: Tracking error results [pure pursuit lateral controller]

Q. Evaluate the performance of the Stanley kinematic and dynamic controllers

The Stanley kinematic controller is mainly suitable for low speeds because it does not make use of a look ahead parameter. The absolute value of the path tracking error is the distance between the center of the vehicle's front wheel P_F and the closest point of the path P_P w.r.t P_F .

$$|e| = \overline{P_F P_P} \quad \text{and} \quad \delta = \delta\theta + \arctan\left(\frac{K_e \cdot e}{v_f}\right) \quad (6.3)$$

To evaluate the Stanley kinematic controller, several tests were conducted using the following variables totalling 27 tests. The results are shown in Figure 6.5 and Table 6.3:

- $u = [20, 30, 40, 50, 60, 70, 80, 90, 100]$ km/h
- Gain $K_e = [0.1, 0.5, 1]$

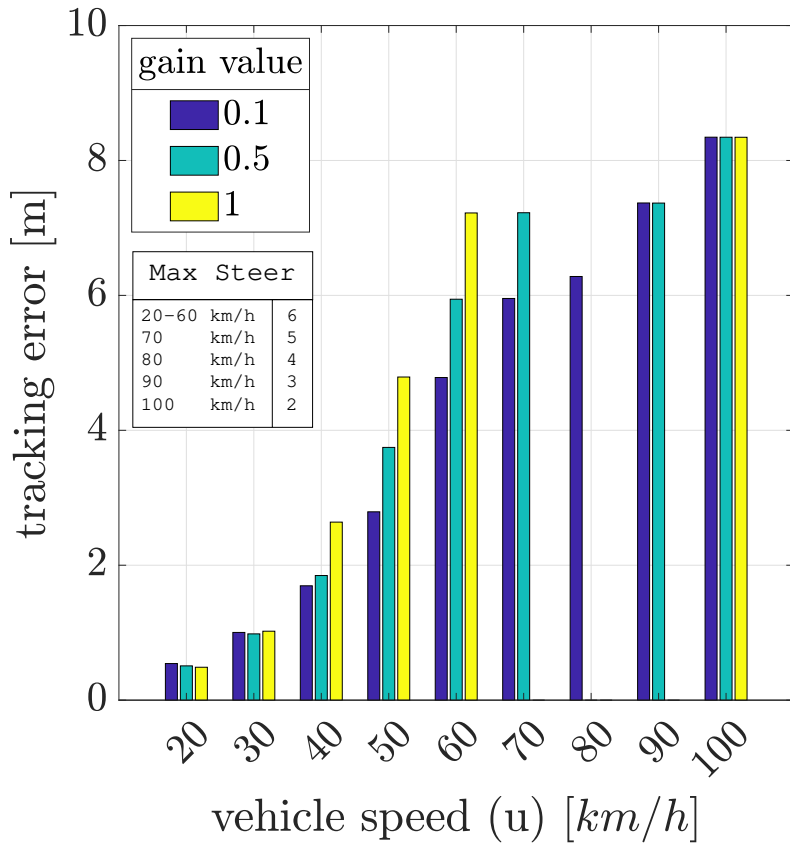


Figure 6.5: Stanley kinematic lateral controller at different u and gain K_e

| u [km/h] | $K_e = 0.1$ | $K_e = 0.5$ | $K_e = 1$ |
|------------|----------------------|----------------------|----------------------|
| 20 | 5.4×10^{-1} | 5.1×10^{-1} | 4.9×10^{-1} |
| 40 | 1.7 | 1.8 | 2.6 |
| 60 | 4.8 | 5.9 | 7.2 |
| 80 | 6.3 | NA | NA |
| 100 | 8.3 | 8.3 | 8.3 |

Table 6.3: Tracking error results [Stanley kinematic lateral controller]

It is important to note that the max steering angle had to be changed for the higher speeds in order for the controller to stabilize the vehicle [shown on Figure 6.5]. As expected, the Stanley kinematic lateral controller works well with lower speeds, and struggles with speeds higher than 60 km/hr for our vehicle.

The Stanley dynamic controller uses a similar equation as the kinematic controller to calculate δ , except it has an extra gain parameter K_y to actively dampen the yaw rate dynamics during high speeds.

$$\delta = \delta\theta + \arctan\left(\frac{K_e \cdot e}{v_f}\right) + K_y(\Omega_t - \Omega) \quad (6.4)$$

The evaluation for the Stanley dynamic lateral controller followed the same test process as the kinematic one. Both gains K_e and K_y were changed simultaneously with the same value for each test. The results are shown in Figure 6.6 and Table 6.4.

Similar to the kinematic controller, the dynamic controller needed smaller maximum steering angles with higher speeds to stabilize the vehicle [shown on Figure 6.6]. However, the overall performance of the dynamic controller was better than the kinematic version.

| u [km/h] | $K_e/K_y = 0.1$ | $K_e/K_y = 0.5$ | $K_e/K_y = 1$ |
|------------|----------------------|-----------------|---------------|
| 20 | 4.3×10^{-1} | 1.1 | 1.3 |
| 40 | 1.4 | 1.4 | 1.4 |
| 60 | 3.4 | 3.6 | 3.6 |
| 80 | 6.3 | 6.3 | 6.3 |
| 100 | 7.8 | 7.8 | 7.8 |

Table 6.4: Tracking error results [Stanley dynamic lateral controller]

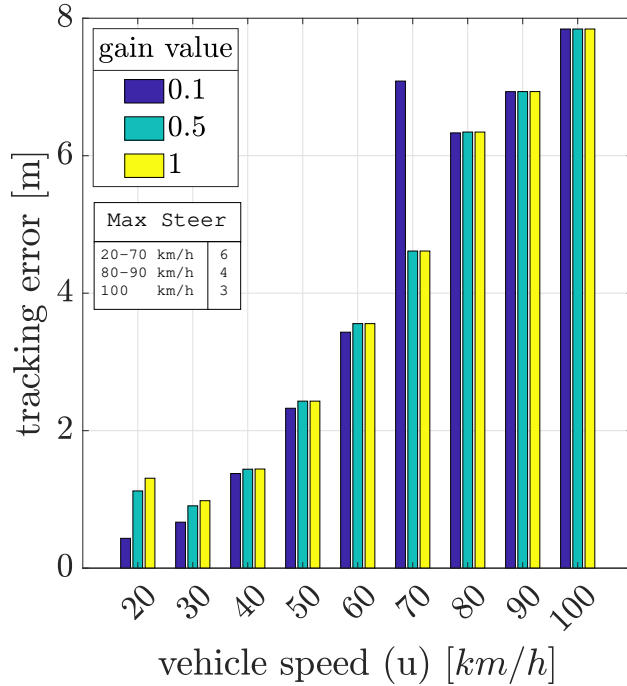


Figure 6.6: Stanley dynamic lateral controller at different u and gain K_e and K_y

Q. Compare the performance of the lateral controllers

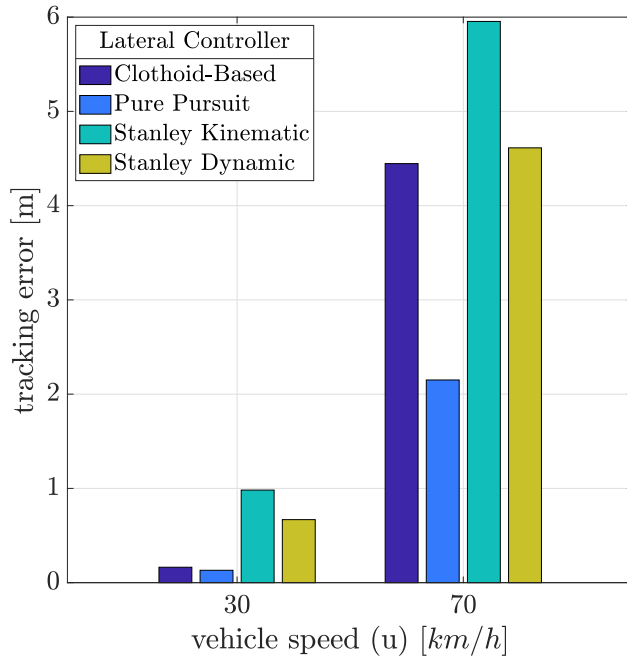


Figure 6.7: Lateral controllers maximum tracking error comparison at different u

The comparison will be based on the maximum tracking error and the steering behaviour. One example of a low speed (30 km/h) and high speed (70 km/h) run were chosen for each

Assignment 6 – Lateral Control

controller. The best performing hyper parameters [look ahead, gains, max steer angle] for each controller were chosen based on the tests previously conducted. The tracking error results are shown in Figure 6.7.

From a tracking error metric prospective, the pure pursuit controller performed the best on both low and high speeds. It was capable of maintaining stability at much higher speeds. As a comparison, pure pursuit was able to achieve target with speeds up to 130 km/hr, while the other controllers had trouble with any speed over 70 km/hr. Furthermore, pure pursuit requires only one hyper-parameter to tune.

On the other side of the spectrum, Stanley Kinematic was the worst performer on both low and high speeds. For both the Stanely controllers, it was no surprise they would not perform well, especially on higher speeds due to the lack of a look ahead feature.

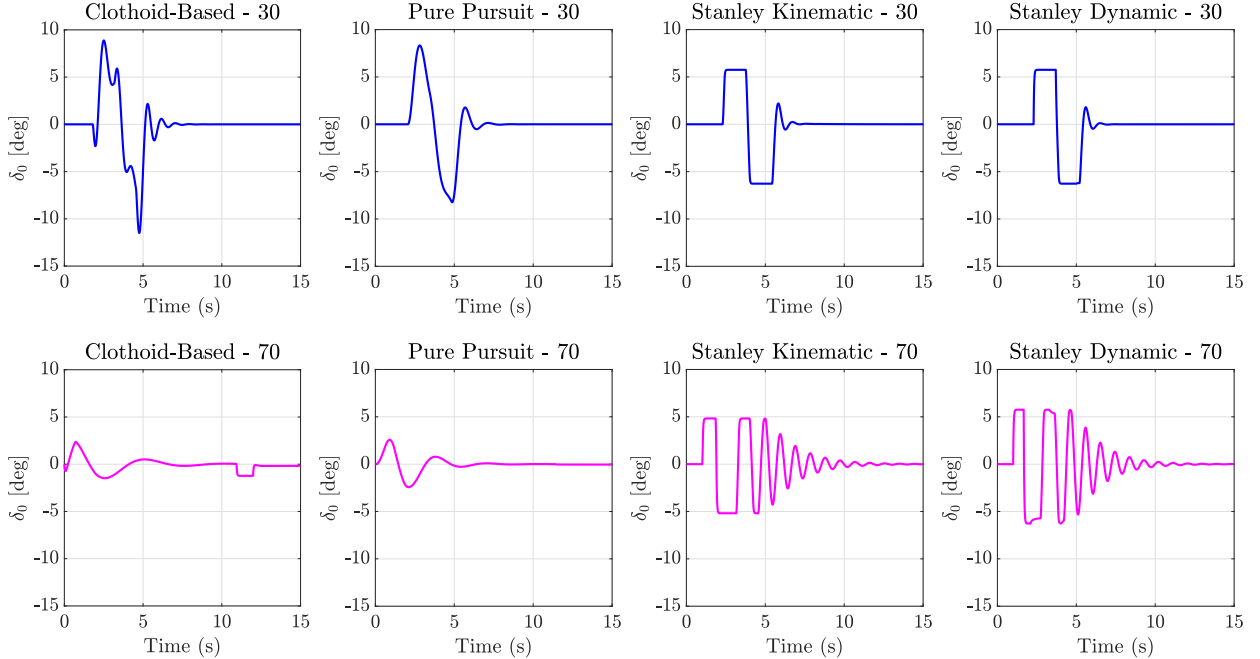


Figure 6.8: Lateral controllers steering behaviour comparison at different u

The steering angles for the same chosen runs are plotted in Figure 6.8. The steering angle for pure pursuit exhibited the best smoothness in steering with no sudden jerky changes. It would be a pleasant ride in a vehicle using this controller.

The clothoid based controller is trailing slightly behind pure pursuit as it showed more sudden transitions between angles, which could make it a less comfortable ride compared to the pure pursuit.

Assignment 6 – Lateral Control

Both of the Stanley controllers showed the same pattern. Some oscillation were present at the higher speed run.

Overall, from a tracking error prospective, and steering behaviour, the pure pursuit lateral controller is a clear winner compared to the rest of the controllers tested.

Q. Underline the pros and cons of each algorithm

| Controller | Pros | Cons |
|----------------|--|---|
| Clothoid-based | <ul style="list-style-type: none"> smooth steering behaviour benefits from knowledge of the vehicle's handling behaviour best overall performer at lower speeds | <ul style="list-style-type: none"> requires 2 hyper parameters high computation cost poor on high speeds |
| Pure pursuit | <ul style="list-style-type: none"> tracks reference very well simple to implement only 1 hyper parameter to tune low computation cost functions at very high speeds | <ul style="list-style-type: none"> look ahead must be specific for each speed |
| S. kinematic | <ul style="list-style-type: none"> low computation cost only 1 hyper parameter simple to implement | <ul style="list-style-type: none"> no look ahead feature doesn't do well in high speeds |
| S. dynamic | <ul style="list-style-type: none"> works better on higher speeds than the kinematic version performs well on low speeds | <ul style="list-style-type: none"> no look ahead feature requires 2 hyper parameters shows oscillations at higher speeds |

Table 6.5: Pros and Cons of lateral controllers

Assignment 7

Motion Planning and Control

7.1 Exercise 1 - route planning

Q. Optimize the route planning task using RRT* algorithm

The optimization included multiple parameters which are listed below along with the values tested for each one:

- **connection distance (c_dist):** decides the maximum distance allowed when sampling for a new vertex. Generated vertices are closer together with shorter distance.
[20, 30, 35, 40, 45, 50, 55, 60 , 70] m
- **number of iterations (itr):** how many times to generate new vertices. Number of generated vertices increase with higher iterations.
[($10^2 \rightarrow 10^3$), ($10^3 \rightarrow 10^4$), ($10^4 \rightarrow 10^5$), ($10^5 \rightarrow 10^6$)]
- **max allowable steering angle (δ):** decides the maximum angle the vehicle can steer.
[4, 5, 6, 7, 8] °
- **interpolation samples:** the space between vertices to sample from. The smaller the number the bigger the sampling pool.
[10, 30, 50, 70, 90]

The optimization metrics are mainly the elapsed time taken to calculate the distance of the generated path, and the smoothness of said path.

Figure 7.1 and Table 7.1 show the time taken for the RRT* to calculate the reference path. The results are categorized based on two variables, the connection distance and the number of iterations of the algorithm.

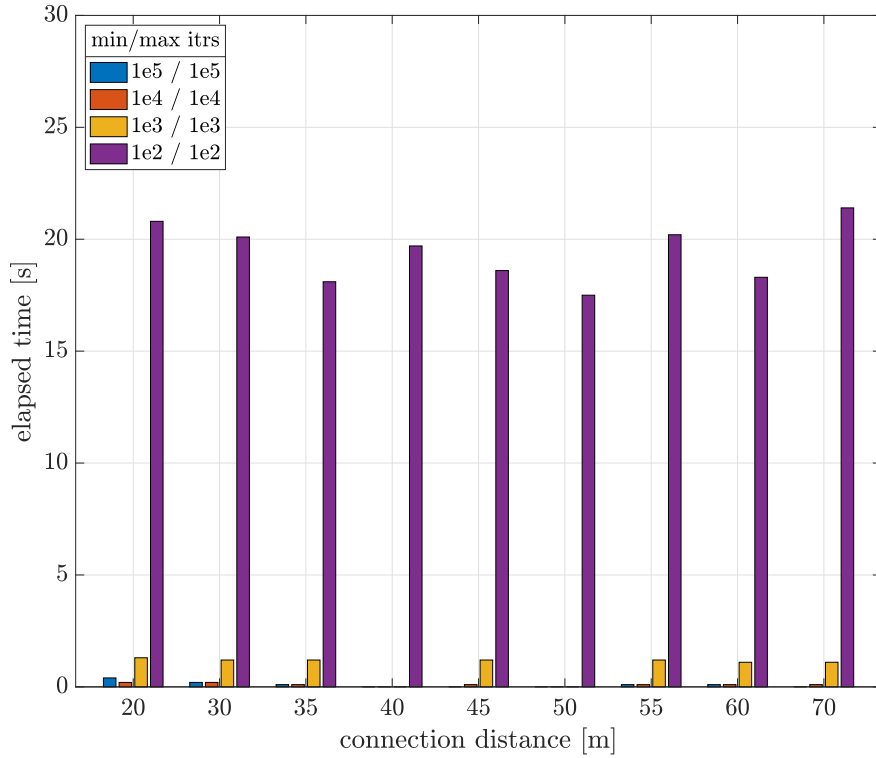


Figure 7.1: combined effect of c_dist and iteration count on elapsed calculation time

It appears that there is no co-relation between the connection distance and elapsed time. The biggest impacting variable on elapsed time is the number of iterations. Going from minimum iteration of 10^4 to 10^5 increased the elapsed time by 20 folds.

| c_dist [m] | itr = 10^2 | itr = 10^3 | itr = 10^4 | itr = 10^5 |
|------------|--------------|--------------|--------------|--------------|
| 20 | 0.4 s | 0.2 s | 1.3 s | 20.8 s |
| 35 | .1 s | .1 s | 1.2 s | 18.1 s |
| 45 | NA | .1 s | 1.2 s | 18.6 s |
| 55 | .1 s | .1 s | 1.2 s | 20.8 s |
| 70 | NA | .1 s | 1.1 s | 21.4 s |

Table 7.1: elapsed time results for connection distance and iteration count]

The resulting paths from RRT* are plotted in Figure 7.2 and 7.4 to further analyse the effect of connection distance and iteration count.

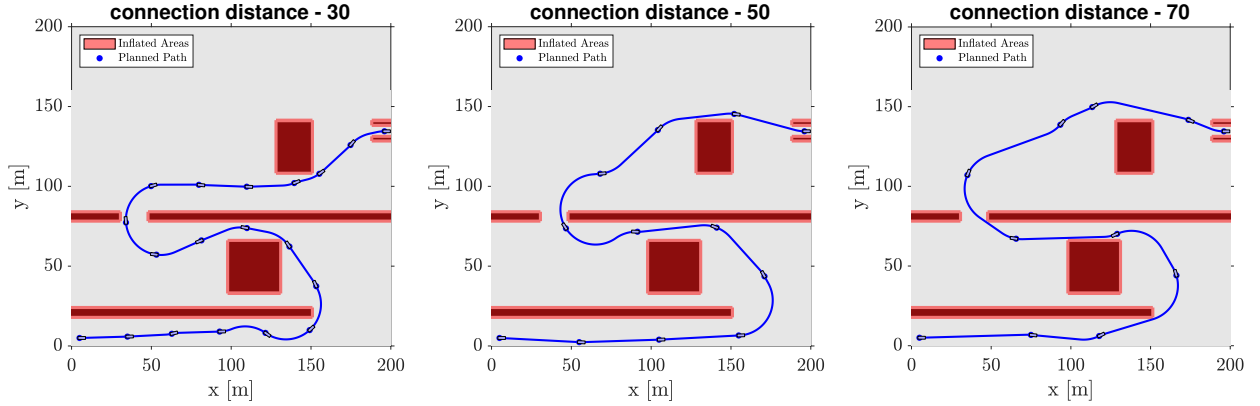


Figure 7.2: connection distance effect on RRT* [min itr = 10^5]

The smaller the connection distance, the closer the vertices on the path. When the distance between vertices are smaller the path appear to have more turns and more steering input.

Decreasing the distance has no major impact from a computational time prospective. However, it could negatively impact the controller's capability of tracking the reference path. As shown in Figure 7.3, with smaller connection distance, the tracking error increases.

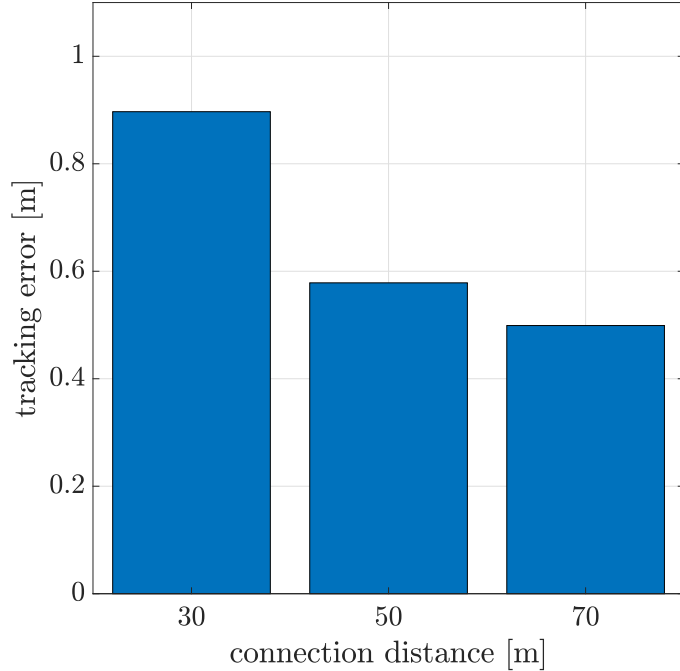


Figure 7.3: Tracking error at 50km/h with different connection distances

Figure 7.4 shows that increasing the iteration count improves the path optimization. Higher iteration count allows RRT* to find a better solution that has a smaller distance. The average distance of the total path for each iteration count was calculated based on 30 different tests and the results are shown in Figure 7.5.

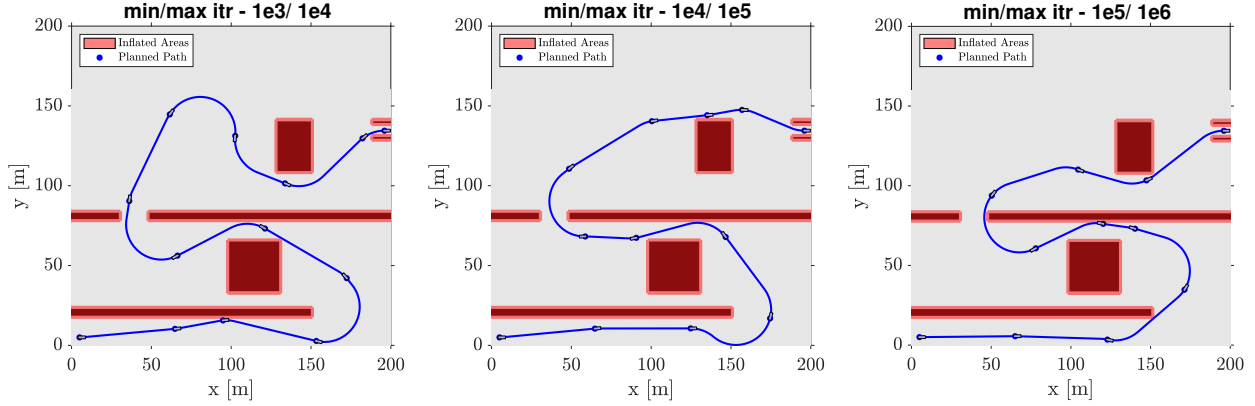


Figure 7.4: number of iterations effect on RRT* [connection distance = 60]

The percent improvement achieved going from minimum iteration of 10^4 to 10^5 is only 2% [533 \rightarrow 524 m]. This was not quite worth it as the elapsed time taken to compute increased 20 times. Therefore, the best minimum/maximum iteration count is $10^4 \rightarrow 10^5$.

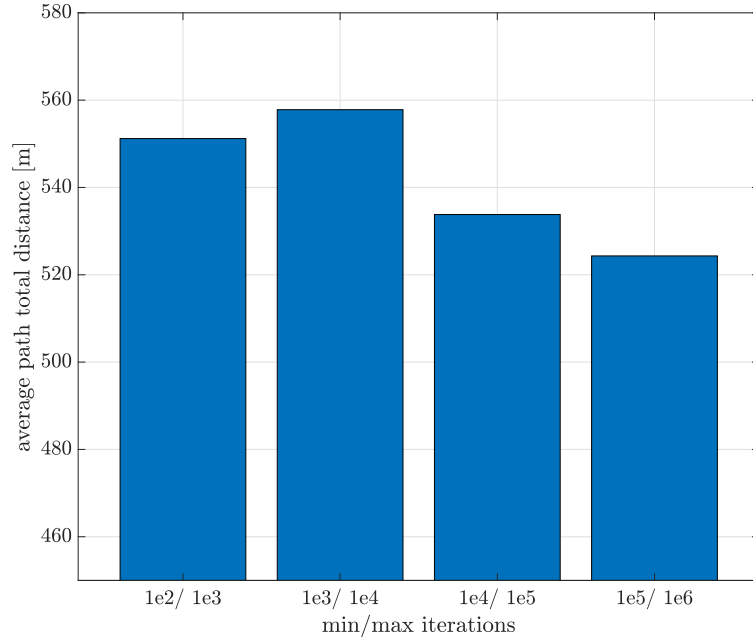


Figure 7.5: Generated path average total distance for each iteration count

The effect of maximum steering angle δ would impact the dynamics of the vehicle much more than RRT*. That is why Figure 7.6 shows the generated path along with the real tracked

path using the clothoid lateral controller optimized previously. The biggest difference in the RRT* generated path is that the radius of curvature can be smaller with larger δ , which in theory should increase the chances of finding a feasible solution.

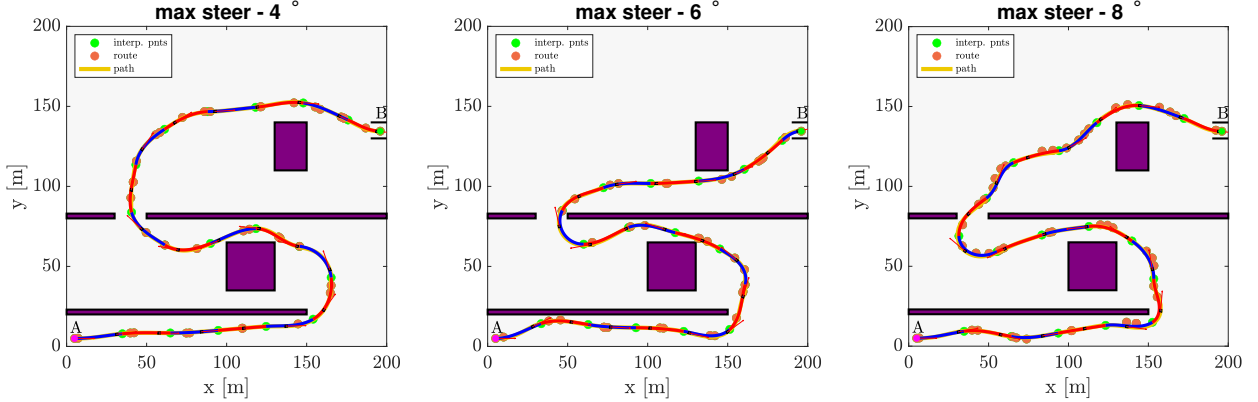


Figure 7.6: $\max \delta$ effect on RRT* and path tracking at 50km/h [min itr = 10^5]

Tracking becomes more difficult with increasing δ , especially with higher speeds. In Figure 7.7, the tracking error was calculated for each steering angle with a velocity $u = 50$ km/h. A max steering angle of 5° is preferred.

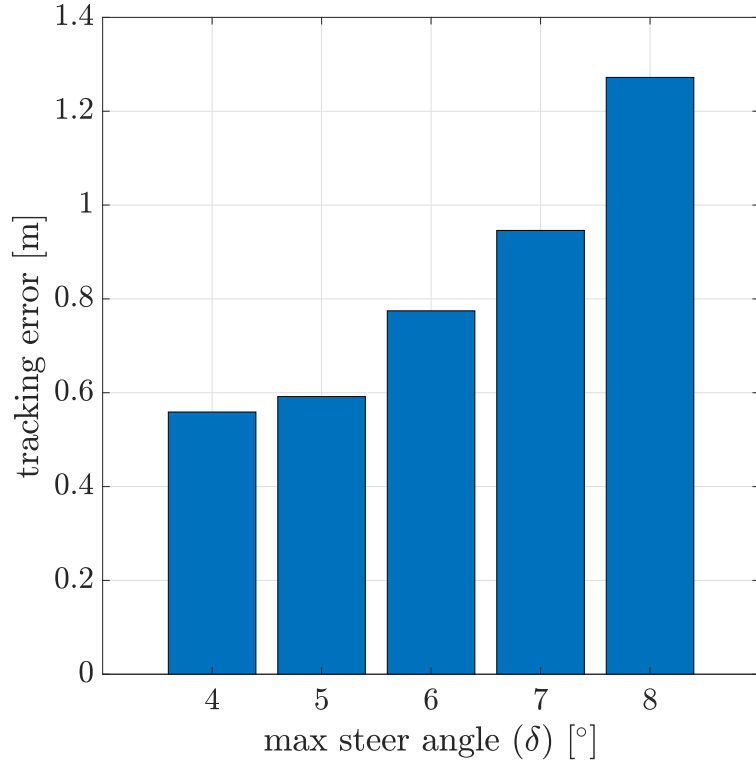


Figure 7.7: Tracking error at 50 km/h with different max δ

Assignment 7 – Motion Planning and Control

The interpolation samples parameter was tested on the same generated route to examine its effect. A route was generated using [$c_dist = 35$, $itr = 10^4$, $\delta = 5^\circ$]. The path was then interpolated with five different numbers in which three of them are shown in Figure 7.8. The resolution of the path [number of vertices] decreases with an increase in the interpolation sample.

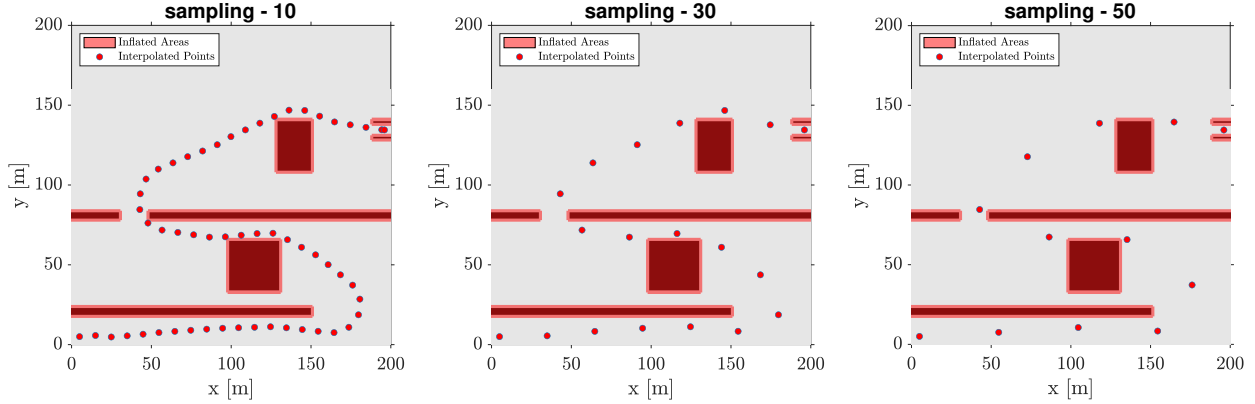


Figure 7.8: Effect of interpolation samples parameter on path resolution

Using the clothoid based lateral controller, the interpolated path for each interpolation sample was tested, and the results are shown in Figure 7.9. The tracked path becomes smoother with higher interpolation sample number, which makes it easier to stabilize the vehicle. This is evident in the tracking error results [Figure 7.10].

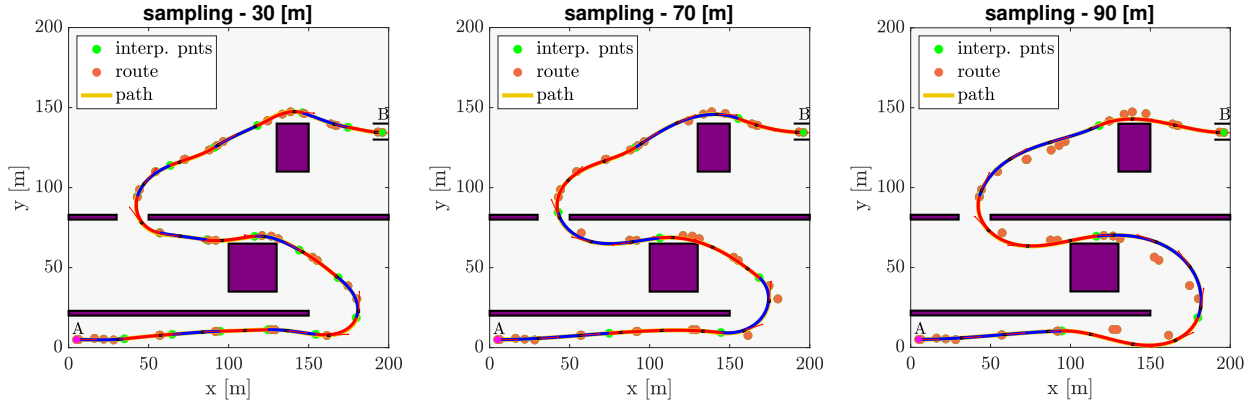


Figure 7.9: Clothoid based controller tracking different interpolation samples

The interpolation sample is a very useful tool to apply. As demonstrated, it smooths out the generated path making it easier for the controller to track it. An ideal interpolation sample for our test would be 50 or 70.

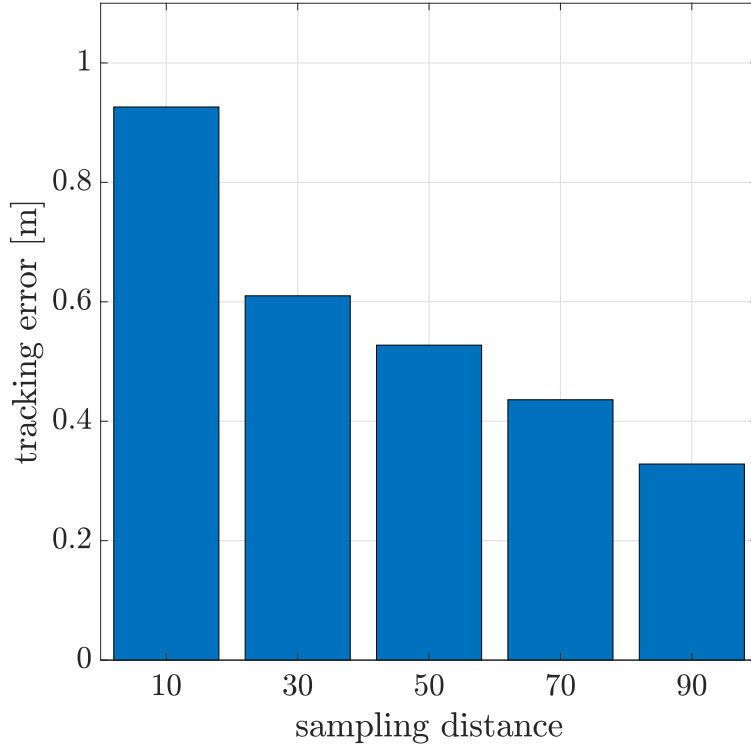


Figure 7.10: Tracking error at 50 km/h with different interpolation sample

Clothoid fitting of the path is better than Dubins path because of the following reasons:

- Dubins path is only limited to three different maneuvers[straight, left or right turns] in six different combinations [RSR, LSL, RSL, LSR, RLR, and LRL].
- All the turns of the Dubins path only have a fixed radius of curvature.

Given the results achieved with the optimized RRT*, it is evident that it is a robust and efficient algorithm. It was able to find a feasible and a nearly optimal solution within seconds [Table 7.1]. The route quality was mostly smooth, however, that could be remedied with clothoid fitting and sample interpolation as was demonstrated in Figure 7.9. Furthermore, RRT* is capable of taking into account the dynamics of the vehicle, however, that could impact it's computational time performance. As a conclusion, RRT* is very well suited for a high level planning algorithm.

During the tracking tests conducted, the vehicle starts and maintains the same speed, until it reaches the parking lot, where it decelerates to 20 km/h. I implemented a simulation auto stopping feature to terminate once the vehicle reaches target destination within a threshold.

Assignment 7 – Motion Planning and Control

In addition, the look ahead starts receding once the remaining distance is smaller than the look ahead value.

A route was generated using [$c_dist = 45$, $itr = 10^4$, $\delta = 5^\circ$], then tested with the clothoid based lateral controller at $u = [30, 50, 70]$. The results of the test are shown in Figure 7.11.

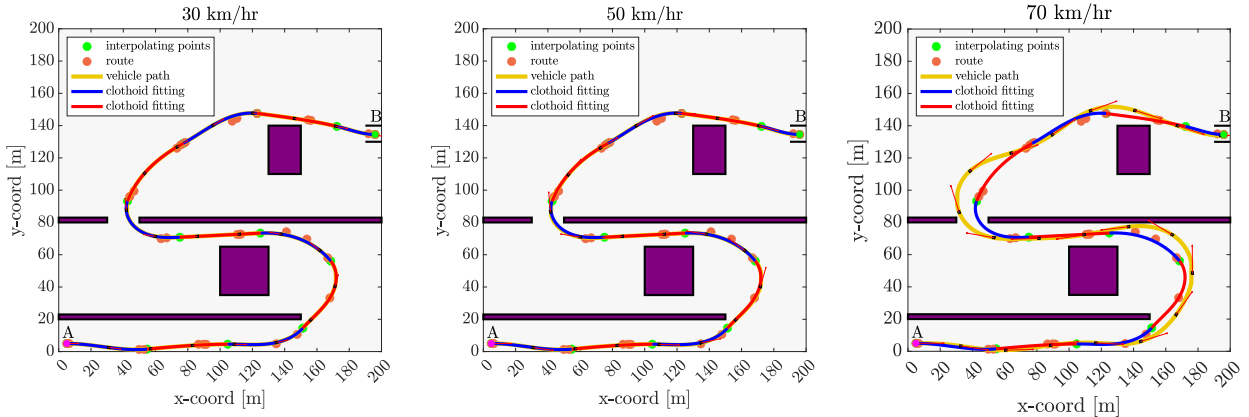


Figure 7.11: Clothoid based lateral controller tracking RRT* result at different speeds

The vehicle tracking worked well with $u = [30, 50]$ km/h. However, tracking error rose significantly at 70 km/h [results are in Figure 7.12]. Summarized results are in Table 7.2.

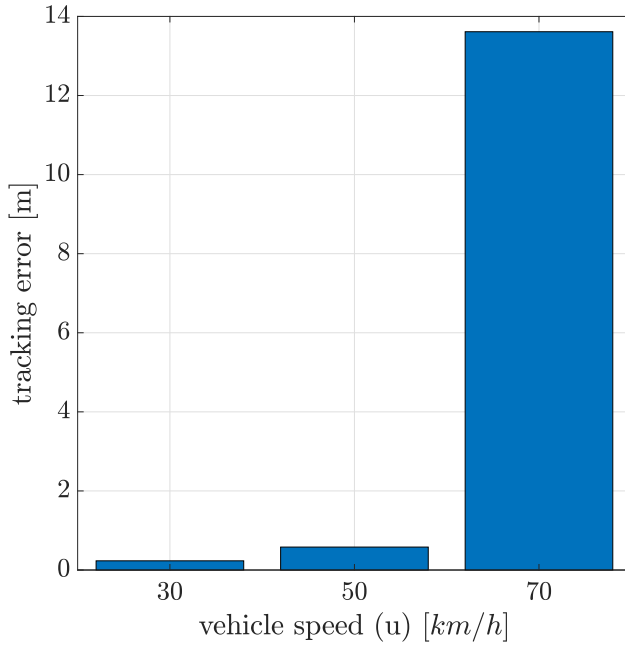


Figure 7.12: Tracking error for clothoid based lateral controller tracking RRT* path

| u [km/h] | tracking time [s] | tracking error [m] | route calculation time [s] |
|------------|-------------------|--------------------|----------------------------|
| 30 | 62.4 | 0.2 | 1.6 |
| 50 | 37.5 | 0.6 | |
| 70 | 28.8 | 13.6 | |

Table 7.2: Route calculation and tracking performance comparison

The time required to calculate the route using RRT* is much shorter than how long it takes to travel the path. This means RRT* can be used in this application to calculate the route online.

The biggest bottleneck for traveling time is certainly the speed at which the car is moving. The higher the speed, the shorter the travel time as shown in Table 7.2. However, the controller's capability falls short at higher speeds causing a major unsafe tracking error.

RRT* could be contributing to the bottleneck if the generated path requires higher steering input. The clothoid fitting alleviates the issue by smoothing out the route and allowing the vehicle to travel faster through turns.

7.2 Exercise 2 - lateral control

The lateral controllers tested earlier will be used on the path that RRT* has generated offline. The controllers will be compared to each other in terms of performance in tracking error, tracking time, and steering behaviour. The list of lateral controllers are as follows:

- Clothoid based lateral control
- Pure pursuit
- Stanley kinematic
- Stanley dynamic

The controllers have already been optimized in the previous chapter and the best resulting parameters are going to be utilized in the following tests.

RRT* generated a reference path offline, and each controller used said reference path for tracking at $u = [30, 50, 60]$ km/h. Results of the tracking error is displayed in Figure 7.13.

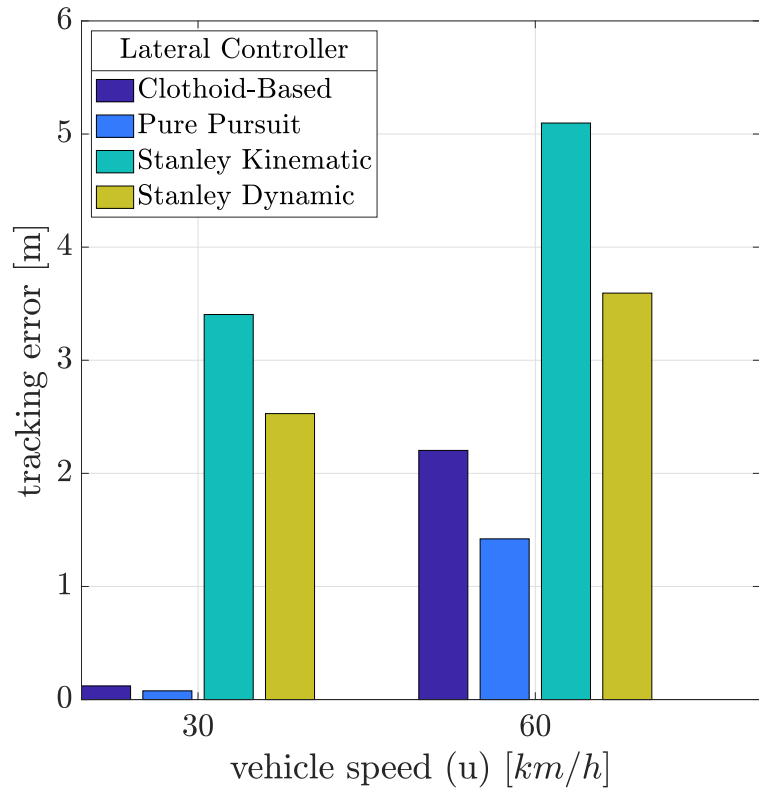


Figure 7.13: Tracking error for lateral controllers following RRT* path

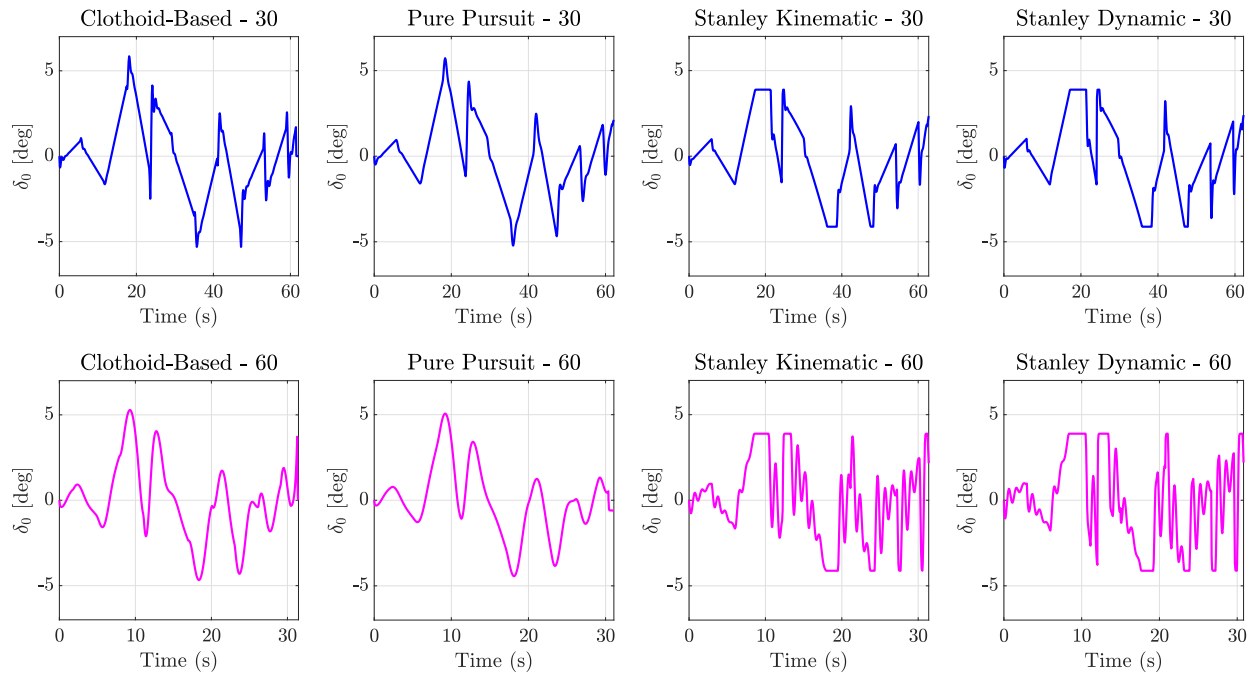


Figure 7.14: lateral controllers steering behaviour following RRT* path

The tests agreed with the previous results achieved in the last chapter. From a tracking error metric prospective, both clothoid based and pure pursuit controllers did well in low speed. However, pure pursuit is much better in higher speeds compared to the rest. Stanley Kinematic struggled on both low and high speeds with the highest tracking error.

Figure 7.14 is the steering behaviour for all the controllers at each speed. The pattern profile for the controllers looked very similar at low speed. Both of the Stanley controllers have a cut off because their max steer parameter is set at 4°.

At the higher speed, pure pursuit seemed to perform the best showing smoother curves. The Stanley controllers struggled and exhibited a lot of oscillations and jitters. The results for the tests are all summarized in table 7.3. The green colored cells highlight the best performer in each category for both speeds.

| Controller | $u = 30 \text{ km/h}$ | | | $u = 60 \text{ km/h}$ | | |
|----------------|-----------------------|--------------|--------------------------|-----------------------|--------------|--------------------------|
| | time [s] | error [m] | total steer input [°] | time [s] | error [m] | total steer input [°] |
| Clothoid-based | 62.0 | 0.12 | 82.6 | 31.4 | 2.20 | 67.2 |
| Pure pursuit | 62.1 | 0.07 | 68.6 | 31.0 | 1.42 | 49.1 |
| S. kinematic | 62.7 | 3.40 | 66.7 | 31.3 | 5.09 | 142.9 |
| S. dynamic | 62.2 | 2.52 | 71.7 | 30.8 | 3.59 | 151.9 |

Table 7.3: Comparison of lateral controllers results

The time taken to get to target is almost identical between the controllers because the bottleneck is the speed of the car. For the tracking error metric, pure pursuit performed best at both low and high speeds.

To put a metric on the steering behaviour, I calculated the total steering input for each run in degrees [results are in Table 7.3]. It was computed by summing the absolute values of the change in steering angle between every two consecutive time steps [equation 7.1].

$$\delta_{tot} = \sum_{n=1}^N |\delta_i - \delta_{i+1}| \quad (7.1)$$

Results agreed with the visual graphs in Figure 7.14, which suggests that pure pursuit had the least amount of total steer input for both low and high speeds, with clothoid based being the second best. A list of the pros and cons for each controller are included in Table 6.5.